Mitochondrial translocation of TFEB regulates complex I and inflammation

Authors: Chiara Calabrese[1,2], Hendrik Nolte[1,2], Melissa R Pitman[3], Raja Ganesan[3], Philipp Lampe[1], Raymond Laboy[1,2], Roberto Ripa[2], Julia Fischer[1,4], Sandhya Chipurupalli[3], Saray Gutierrez[1], Ruhi Polara[3], Daniel Thomas[5], Stuart M Pitson[3], Adam Antebi[1,2,6] and Nirmal Robinson [1,3,6]

[1]Cologne Excellence Cluster on Cellular Stress Responses in Aging-Associated Diseases (CECAD), University of Cologne, Cologne, Germany

[2]Max Planck Institute for Biology of Ageing, Cologne, Germany

[3]Centre for Cancer Biology, University of South Australia and SA Pathology, Australia

[4]Centre for Molecular Medicine Cologne, Cologne, Germany

[5]Adelaide Medical School, University of Adelaide & Precision Medicine Theme, South Australian Health and Medical Research Institute, Australia

[6]Correspondence should be addressed to N.R. or A.A. (e-mail: Nirmal.Robinson@unisa.edu.au or aantebi@age.mpg.de)

Abstract: TFEB is a master regulator of autophagy, lysosome biogenesis and mitochondrial metabolism that works, and immunity, primarily through transcription controlled by cytosol-to-nuclear translocation. Emerging data indicate additional regulatory interactions at the surface of organelles such as lysosomes. Here we show that TFEB has a non-transcriptional role in mitochondria, regulating the electron transport chain complex I to down-modulate inflammation. Proteomic analysis revealed extensive TFEB co-precipitation with several mitochondrial proteins, whose interactions are disrupted upon infection with *S.* Typhimurium. Localization of TFEB in the mitochondrial matrix was confirmed by high resolution confocal microscopy and biochemistry with translocation dependent on a conserved N-terminal TOMM20-binding motif enhanced by mTOR inhibition. Within the mitochondria, TFEB and protease LONP1 antagonistically co-regulate complex I, reactive oxygen species and the inflammatory response. Consequently, during infection, lack of TFEB specifically in the mitochondria exacerbates the expression of pro-inflammatory cytokines, contributing to innate immune pathogenesis.

Introduction

The transcription factor EB (TFEB) is a key regulator of autophagy, lysosomal biogenesis and cellular metabolism (Lapierre *et al*, 2013; Napolitano & Ballabio, 2016; Settembre & Ballabio, 2011) with increasingly recognized roles in the regulation of innate immunity (Irazoqui, 2020). TFEB nuclear activity is dependent on the mechanistic target of rapamycin (mTOR), which under nutrient-rich conditions, phosphorylates TFEB at Ser 122, Ser142 and Ser211 facilitating binding to 14-3-3 adaptor proteins, and preventing its nuclear translocation and transcriptional activity (Martina *et al*, 2012). Conversely, mTOR inhibition during lysosomal stress and

starvation results in reduced TFEB phosphorylation, permitting its nuclear translocation and transcriptional function (Settembre *et al*, 2012b). TFEB has also been shown to co-localize with mTOR on the surface of lysosomes, in a RAG GTPase-dependent manner (Settembre *et al.*, 2012b) serving as a lysosomal "sensor" in addition its established role as a lysosomal transcriptional "effector".

Mitochondrial function is maintained via a balance of biogenesis, fission, fusion and specific autophagy (mitophagy). Mitophagy is partially regulated by TFEB (Nezich *et al*, 2015; Zhang *et al*, 2016), especially in response to mitochondrial stress such as that induced by electron transport chain inhibition and induces TFEB-dependent expression of mitophagy receptors Ndp52 and Optn. Beta islet cell specific knockout of TFEB abrogated high-fat diet-induced mitophagy with increased reactive oxygen species (ROS) production (Park *et al*, 2022), indicating a critical link between mitochondrial electron transport complex function and TFEB. Moreover, TFEB transcriptionally regulates genes involved in mitochondrial biogenesis and glucose uptake (Mansueto *et al*, 2017) and loss of TFEB results in accumulation of morphologically abnormal and dysfunctional mitochondria (Mansueto *et al.*, 2017). More recently, TFEB has been reported to induce mitochondrial itaconate production in macrophages, which inhibits bacterial growth (Schuster *et al*, 2022) and regulates extrusion of mitochondrial contents in hepatocytes exposed to lipopolysaccharide (Unuma *et al*, 2015) but, direct non-transcriptional roles of TFEB on mitochondrial function have not been identified.

Effective upregulation of autophagosomes and lysosomes via TFEB is required for xenophagy and the destruction of intracellular pathogens such as *Mycobacteria* (PMID

(Ouimet *et al*, 2016)) and *Salmonella* (Schuster *et al.*, 2022), constituting an essential innate immune response. TFEB regulates inflammation and immunity upon infection in macrophages in a transcriptional program conserved in the nematode *Caenorhabditis elegans* (Pastore *et al*, 2016; Visvikis *et al*, 2014) with recent data indicating mitochondrial metabolism may contribute to the effector function of TFEB activated macrophages (Schuster *et al.*, 2022).

Here we report that TFEB has a previously unknown mitochondria-specific function. We have established that TFEB translocates to mitochondria via a TOMM20-binding motif forming a complex with LONP1 to regulate electron transport complex I. Our observations show a direct link between mitochondrial ROS production and innate immune defense regulated directly by TFEB.

Results

TFEB localizes to the mitochondrial matrix

To identify novel functions of TFEB in an unbiased manner, we performed high affinity mass spectrometry to identify proteins interacting with ectopically expressed TFEB in uninfected cells vs *S.* Typhimurium-infected or torin-1-treated cells. We investigated *S.* Typhimurium infection as we had previously shown this pathogen activates mTOR, prevents autophagy and induces inflammation (Ganesan *et al*, 2017). Significant interacting partners were determined by two-tailed t-test and then corrected for multiple testing by permutation-based FDR estimation (FDR < 0.05) (Figure S1A) In total, we identified 79 proteins that showed 2-fold upregulation in untreated conditions. As expected, 15 core candidates including 14-3-3 proteins (YWHAQ, YWHAB, YWHAG, YWHAE, YWHAZ, YWHAH) which are well established binding

partners of TFEB (Xu *et al*, 2019) were significantly 2-fold upregulated compared to control in all treatments, validating our immunoprecipitation results (Figure 1A, Supplementary Table 1, Figure S1B). As expected, (Xu *et al.*, 2019) the intensity of TFEB binding with 14-3-3 proteins were reduced upon torin-1 treatment (Figures 1A and S1B).

We then selected proteins that were significantly upregulated at least 2-fold in any treatment. This set contains 130 proteins indicating a highly dynamic TFEB interactome (Supplementary Table 1). Strikingly, 28 out of 130 proteins localized to the mitochondria, including ATAD3B, LRPPRC, HSPA1B, and HSPA9 (Figure 1B and 1C). The majority of proteins (75 out of 130) were associated with the nucleus (Figures 1B) including TFEB, STAT3, PSMA4 and these interactions were mostly maintained in untreated (UT) conditions and upon torin-1 treatment but reduced upon *S*. Typhimurium (ST) infection (Figure 1C). Taken together, these data suggested a potential localization and function of TFEB in mitochondria.

Consistent with this notion, confocal microscopy indicated that endogenous TFEB colocalized with ectopically expressed TOMM20-GFP, a mitochondrial import receptor subunit that aids passage of proteins into the mitochondrial matrix (Figure 1D). The Manders co-localization coefficient (tM1) for TOMM20-GFP was 0.2057 and for TFEB (tM2) was 0.1723 (Figure 1E), indicating significant overlap as quantified by colocalization imageJ analysis. We then established a HeLa cell line in which TFEB was stably depleted by shRNA (shTFEB) (Figures S1C and S1D). Cell fractionation of shRNA control (shCTRL) and shTFEB followed by Western blotting showed the presence of TFEB in the mitochondrial fraction from shCTRL but not shTFEB cells

(Figures 1F and 1G). As previously reported (Settembre *et al*, 2011b), autophagy was inhibited in TFEB-depleted cells, as the levels of the autophagy marker LC3B is decreased both at the basal level and upon torin-1 treatment (Figure S1E). We also isolated mitochondria from HEK cells using anti-TOM22 microbeads, which yielded highly enriched mitochondria (TOMM20) devoid of contaminants from endoplasmic reticulum (ER) (PDI), cytoplasm (GAPDH) and nucleus (LAMIN B). Notably, TFEB was found to be enriched in mitochondrial fraction (Figure 1H) and was not specific to cancer cell lines as we also detected TFEB in the mitochondrial fraction of primary human monocyte derived macrophages (Figure S1F).

Immunofluorescence stimulated emission depletion (STED) microscopy revealed that TFEB was in close proximity with mtDNA (Figure 2A) and the mitochondrial DNA staining was confirmed to be present in TOMM20-stained mitochondria (Figure S2A). To identify more precisely the localization of TFEB within the mitochondria, we performed protease protection assays on mitochondria isolated from HeLa cells (Figures 2B and 2C). In the absence of swelling buffer, trypsin degraded the outer mitochondrial membrane (OMM) protein TOMM20. In the presence of swelling buffer, trypsin degraded the inner mitochondrial membrane (IMM) protein TIM23. By contrast, the matrix protein SLP2 was resistant to trypsin digestion, TFEB was partially degraded suggesting that it could be partially present on the inner membrane but primarily localized within the mitochondrial matrix. However, TFEB was not resistant to trypsin *per se*, as both TFEB and SLP2 were digested by trypsin when the mitochondria were incubated with triton X-100. We also confirmed that TFEB was localized to the mitochondrial matrix in HEK293 cells (Figures S2B and S2C). Additionally, immunogold labelling of TFEB followed by transmission electron microscopy (TEM)

detected gold particles in contact with the mitochondrial cristae, as well as the nucleus and cytoplasm (Figures 2D and 2E). Mitochondrial import assays using ^{35}S radiolabeled TFEB translated *ex vivo* further demonstrated that TFEB was actively imported into mitochondria in a membrane-potential-dependent manner as CCCP
155 treatment significantly reduced TFEB translocation into mitochondria (Figure 2F and 2G).

Mitochondrial localization signal (MLS) of TFEB enables mitochondrial translocation

The majority of the proteins destined to the mitochondrial matrix are synthesized
160 with matrix-targeting sequences (MTS) (Backes & Herrmann, 2017). We predicted a putative MTS for TFEB using MitoProt II (https://ihg.gsf.de/ihg/mitoprot.html) and generated a TFEB construct in which we deleted the putative MTS (ΔMTS) to assess whether this domain is responsible for its mitochondrial translocation. Cell fractionation performed on HeLa cells expressing an empty FLAG plasmid, FLAG-tagged WT-TFEB
165 or FLAG-tagged ΔMTS-TFEB (Figures S3A and S3B), however, the ΔMTS-TFEB translocated into the mitochondria, indicating that translocation is independent of the predicted MTS (data not shown). We also identified a specific TOMM20 binding consensus motif (VMHYM) in TFEB using MitoProt II (http://mitf.cbrc.jp/MitoFates/cgi-bin/top.cgi), which we termed as the mitochondrial localization sequence (MLS). To
170 test whether this motif directed TFEB translocation into mitochondria, we mutated the MLS from the WT-TFEB plasmid (aa 30 from V to K) by site directed mutagenesis to change the charge (Figure 3A). Cell fractionation analyses on HeLa cells expressing MLS-TFEB revealed that the mutated MLS prevented TFEB translocation to the mitochondria (Figures 3B and S3C), and mitochondrial import of ^{35}S radiolabeled MLS-

175 TFEB translated *ex vivo* showed an impairment in mitochondrial translocation, further demonstrating the function of the MLS motif in mitochondrial import (Figure 3C). Immunofluorescence staining of HeLa cells showed that endogenous TFEB and TOMM20 colocalized (Figure S3D). Manders co-localization coefficients for TFEB and TOMM20 were found to be (tM1) 0.1652 and (tM2) 0.2245, respectively (Figure S3E).
180 TFEB co-localization with TOMM20 was also tested and quantified for both WT-TFEB FLAG and the mutant MLS-TFEB FLAG. We observed increased co-localization of WT-TFEB FLAG with TOMM20 (with a Manders co-localization coefficient of 0.2016) compared to the MLS-TFEB plasmid (with a Manders co-localization coefficient of 0.1030). However, no difference in nuclear localization was detected between the WT-
185 TFEB and the mutant MLS-TFEB as the Manders co-localization coefficients between the FLAG signal and DAPI were 0.3953 and 0.3190 respectively (Figure S3F). We found that the TOMM20 binding motif is conserved in higher mammals, but not present in zebrafish or *C. elegans* (Figure 3D). In line with this, the *C. elegans* TFEB orthologue, HLH-30, was not found to reside in mitochondria (Figure S3G).

190 Because lysosomal biogenesis is a crucial transcriptional function of TFEB (Settembre *et al*, 2011a) we asked whether the MLS mutant preserved TFEB transcriptional activity by analyzing the mRNA of its lysosomal target genes. Reduced target gene expression in shTFEB was rescued when the cells were reconstituted with either WT-TFEB or MLS-TFEB mutant plasmids (Figure 3E), indicating that TFEB
195 transcriptional activity is uncompromised in the MLS-TFEB transfected cells.

Mitochondrial translocation of TFEB is mTOR-dependent

As TFEB nuclear translocation is mTOR-dependent (Settembre *et al*, 2012a), we investigated whether TFEB mitochondrial localization also shows mTOR regulation. Inhibition of mTOR using torin-1 in HeLa cells increased the global expression of TFEB and its nuclear translocation as TFEB is also known to autoregulate itself (Settembre *et al*, 2013), but also promoted TFEB mitochondrial translocation (Figures 3F and 3G).

This finding is consistent with our mass spectrometry analysis (Figure 1C), in which we observed a positive interaction between TFEB and a subset of mitochondrial proteins upon torin-1-treatment. TFEB subcellular localization is known to be mediated by mTOR-dependent phosphorylation of TFEB residues Ser122, Ser142, and Ser211 (Settembre & Ballabio, 2011). We next investigated the phosphorylation status of TFEB in mitochondria (M) to the total cell lysate (C) in HeLa cells by mass spectrometry. This analysis revealed that the pool of TFEB present in the mitochondria was not phosphorylated on the identified phosphorylation sites colored in red (Ser122, Ser332 and Ser334) (Figure 3H). Ser467 was the only phosphorylated residue to be detected in the mitochondria pool, which is known to be responsible for TFEB cytosolic stabilization, as it prevents TFEB nuclear translocation independently of mTORC1 (Palmieri *et al*, 2017). The phosphorylation of TFEB on these Ser residues was lost upon torin-1 treatment (Figure 3H). Furthermore, upon torin-1 treatment, TOMM20 co-immunoprecipitated with endogenous TFEB (Figure 3I). These data suggest that inhibition of mTOR allows the translocation of the dephosphorylated pool of TFEB into mitochondria, which is dependent on the identified MLS motif.

Loss of TFEB disrupts mitochondrial morphology and function

Next, we studied whether mitochondrial morphology and function were affected upon TFEB depletion. (Settembre *et al.*, 2011b) We observed that the mitochondrial network was altered, as mitochondria clustered asymmetrically in the perinuclear region in TFEB-depleted cells (Figures 4A and S4A). The mitochondrial network was rescued
225 with ectopic expression of WT-TFEB but not when complemented with the MLS-TFEB mutant (Figure 4B). TFEB mitochondrial localization and altered mitochondrial morphology in TFEB-depleted cells, prompted us to investigate the impact of TFEB on mitochondrial respiration (Figure 4C). Seahorse analysis showed increased Basal respiration, ATP-linked respiration, and Maximal respiration in shTFEB, which dropped
230 to baseline when cells were reconstituted with WT-TFEB, but not with the MLS-TFEB mutant (Figure 4D). Consistently, increased ATP-linked respiration and Maximal respiration was observed also in HEK293T cells when transiently transfected with siRNA against TFEB compared to siCTRL (Figure S4B). Taken together, these data indicate that TFEB has a mitochondria-specific function in regulating mitochondrial
235 oxidative phosphorylation.

To better dissect the mitochondria specific functions of TFEB, we generated plasmids which express various mutant forms of TFEB. TFEB not able to translocate to the nucleus (ΔNLS-TFEB) was created by removing the nuclear localization signal (NLS) motif (in which the basic arginine residues R245–R248 were mutated to alanine). TFEB
240 that exclusively localizes in the nucleus was generated by mutating the previously reported serine residues (S142A/S211A) to alanine (Napolitano *et al*, 2018; Roczniak-Ferguson *et al*, 2012). Both constructs were additionally mutated in the identified MLS motif to prevent their mitochondrial translocation (Figure S4C). Subcellular fractionation and confocal microscopy confirmed the cytosolic localization of the ΔNLS-

245 TFEB mutant and the nuclear localization of the S142A/S211A TFEB mutant (Figures S4D and S4E).

We next complemented shTFEB with the generated TFEB plasmids and evaluated their ability to restore mitochondrial function. Interestingly, Basal respiration, ATP-linked respiration and Maximal respiration were rescued in shTFEB cells when
250 complemented with WT-TFEB, but not when complemented with the ΔNLS-TFEB or S142A/S211A-TFEB (Figures S4F and S4G). These data indicate that mitochondrial respiration is regulated by mitochondria localized TFEB.

Mitochondrial complex I assembly is altered in TFEB-depleted cells

To understand how mitochondrial TFEB regulates mitochondrial functions, we
255 performed label-free proteomics on enriched mitochondria from shCTRL and shTFEB to determine the altered expression of mitochondrial proteins. 1D enrichment of Gene Ontology (GO) terms was performed along the $\log_2$ shTFEB/shCTRL ratio to identify up- or down-regulated proteins annotated with the same GO term. Proteins annotated as *mitochondrial respiratory chain complex I* were upregulated in shTFEB compared
260 to shCTRL (Figures 5A and S5A, B). Complex I subunits were plotted based on their localization and modules (Wirth *et al*, 2016) to see whether subunits pertaining to a specific complex I module were altered. We found an overall increase in the expression of complex I subunits in TFEB-depleted cells, unlinked to a specific complex I module (Figure S5C).

265 We next investigated complex I by blue native-polyacrylamide gel electrophoresis (BN-PAGE) and found an increased complex I in shTFEB compared to shCTRL (Figure 5B). We used the mitochondria isolated from the same cells to investigate complex I activity in response to the complex I substrates NADH and Nitro

Blue Tetrazolium (NBT). Complex I activity was also modestly increased in shTFEB
270 compared to shCTRL (Figure 5C). Further, steady state levels of several complex I subunits such as NDUFS5, NDUFA8 and NDUFB10, but not NDUFA9 were higher in the mitochondria isolated from shTFEB than shCTRL (Figures 5D and 5E). We also determined the levels of subunits of other ETC complexes (Figure S5D and S5E) and found that expression of proteins belonging to complex II were also affected in TFEB-
275 depleted cells. SDHA was increased in TFEB-depleted cells, whereas SHDB was decreased. Given that SDHA is also part of the TCA cycle, changes in this protein could also be due to a different metabolic profile of TFEB-depleted cells. However, expression of complex III (UQCRC2), complex IV (COX2) and complex V (ATP5a and ATP5b) associated proteins were not altered in enriched mitochondria of TFEB-
280 depleted cells compared to shCTRL (Figure S5D and S5E).

To test whether the increase in these specific complex I subunits was dependent on mitochondrial TFEB, we studied the expression of NDUFB10 and NDUFA8 in shTFEB cells complemented with WT-TFEB or MLS-TFEB mutant (Figures 5F and 5G). Expression of complex I subunits was reduced when shTFEB cells were reconstituted
285 with WT-TFEB but not with the MLS-TFEB mutant. Collectively, these findings suggest that TFEB-regulated complex I function is mitochondria-specific.

TFEB and LONP1 co-regulate complex I

Turnover of mitochondrial complexes are regulated by chaperones and
290 mitochondrial proteases (Bohovych *et al*, 2015) . Previous studies have shown that the serine mitochondrial protease LONP1 controls complex I by regulating its subunits (Pinti *et al*, 2016). Our proteomics approach also identified LONP1 as one of the interactors that immunoprecipitated with TFEB (Supplementary Table 1) although it

was not detected as one of the top hits. Given the effects of TFEB on complex I, we
295 assessed LONP1 expression levels in TFEB-depleted cells. Interestingly, we observed that TFEB knockdown by siRNA increased LONP1 steady-state protein levels; conversely, depletion of LONP1 (Figures 6A and 6B) or pharmacological inhibition using CDDO (Figure S6A and S6B) increased TFEB expression, showing mutual antagonistic regulation. We observed that depleting LONP1 was sufficient to suppress
300 NDUFB10 and NDUFA8 expression in TFEB-depleted cells (Figures 6A and 6B), but not of other complex I subunits such as NDUFA9 and NDUFS5 (Figures 6C and S6C). LONP1 mRNA levels were not significantly changed in cells depleted of TFEB using TFEB-specific siRNA or shRNA (Figure 6D and S6D), indicating a post-transcriptional regulation. No significant differences were found in the mRNA levels of these subunits
305 upon LONP1 knockdown in shCTRL and shTFEB cells (Figure S6E). These data indicate that TFEB and LONP1 post-transcriptionally modulate complex I function, by regulating specific subunits known to be upregulated upon LONP1 overexpression (Pinti *et al.*, 2016). Next, we asked if the altered OXPHOS in shTFEB is dependent on LONP1 by silencing LONP1. Interestingly, depleting LONP1 was sufficient to restore
310 normal levels of ATP-linked and maximal respiration in TFEB-depleted cells (Figures 6E and 6F). Thus, TFEB and LONP1 cooperatively modulate mitochondrial oxidative phosphorylation.

These data prompted us to investigate whether TFEB and LONP1 form a complex to regulate complex I. We observed that LONP1 immunoprecipitated with
315 endogenous TFEB in HeLa cells (Figure 6G). Ectopically expressed LONP1-HA also co-immunoprecipitated with TFEB-FLAG in HEK293T cells (Figure 6H). TFEB-FLAG expression was reduced in the presence of LONP1-HA when compared to TFEB-FLAG expression as control, further indicating a reciprocal regulation of these two

proteins (Figure 6H). Finally, we purified recombinant LONP1-HA and identified a
320 direct interaction when the protein was incubated with TFEB-FLAG beads (Figure 6I). The purified proteins (LONP1-HA and TFEB-FLAG) were free of contaminants as assessed by SyproRuby staining after SDS-PAGE (Figure S6F). Taken together these data demonstrate that TFEB-LONP1 complex regulates complex I, and therefore mitochondrial function.

325

Mitochondrial TFEB regulates inflammation upon *S.* Typhimurium-infection

Previously, we had shown that *Salmonella* Typhimurium prevents autophagy, disrupts mitochondria (Hos *et al*, 2017), induces inflammation and triggers phenotypes reminiscent of TFEB loss. Therefore, we surmised that TFEB may be dysregulated
330 during *S.* Typhimurium infection. We first asked whether TFEB translocation is affected upon *S.* Typhimurium infection. Immunofluorescence microscopy showed that *S.* Typhimurium prevented TFEB nuclear translocation, however, inhibition of mTOR using torin-1 enabled nuclear translocation as expected (Figures S7A and S7B). We next evaluated TFEB mitochondrial localization upon *S.* Typhimurium infection. Cell
335 fractionation analyses revealed that TFEB accumulated in the cytosol, however, it was absent from the mitochondria (Figures 7A and 7B). These findings are consistent with our data indicating that upon *S.* Typhimurium infection, interactions between TFEB and mitochondrial proteins are lost (Figure 1E) but preserved with 14-3-3 proteins (Figure S1B).

340 TFEB has been shown to transcriptionally regulate cytokine expression during infection (Visvikis *et al.*, 2014); thus, we next asked whether TFEB cytosolic localization affects the inflammatory outcome during *S.* Typhimurium infection. Depletion of TFEB using shRNA resulted in higher IL-6 (Figure 7C) and IL-8 (Figure

7D) secretion compared to control cells in which localization of endogenous TFEB was limited to the cytosol during *S.* Typhimurium infection (Figures S7A and S7B). Consistently, mRNA levels of IL-6, IL-8 and IL-1α were significantly up-regulated in TFEB-depleted cells (Figure S7C).

As TFEB-depleted cells showed increased inflammation (Figures 7C, D and S7C), we investigated whether this behavior is dependent on TFEB mitochondrial localization. Although, *S.* Typhimurium prevented TFEB mitochondrial translocation, ectopic overexpression of WT-TFEB resulted in TFEB mitochondrial localization in shCTRL and shTFEB even in the presence of the bacteria (Figure S7D). Therefore, transiently transfected shCTRL and shTFEB cells with WT-TFEB or MLS-TFEB mutant were infected with *S.* Typhimurium for 24 h and the supernatants analyzed for IL-6. WT-TFEB but not MLS-TFEB mutant expression reduced IL-6 expression in shTFEB (Figure 7E), suggesting that TFEB-mediated regulation of inflammation depends also on its mitochondrial localization. Cytokine expression was also analyzed in shTFEB cells complemented with nuclear TFEB (S142A/S211A) and cytosolic (ΔNLS TFEB). Nuclear TFEB further increased *S.* Typhimurium-induced inflammation possibly due to its increased transcriptional activation of inflammatory cytokines consistent with previous reports (Brady *et al*, 2018; Pastore *et al.*, 2016). However, cytosolic TFEB (ΔNLS TFEB) neither restored nor increased the expression of inflammatory cytokines (Figure S7E).

As mitochondrial Reactive Oxygen Species (mtROS) is one of the key factors that regulate inflammation (Naik & Dixit, 2011), we tested whether this could represent one of the causes of increased inflammation observed in TFEB-depleted cells. mtROS produced upon *S.* Typhimurium infection were analyzed by flow cytometry and found to be increased in TFEB-depleted cells compared to control cells and reduced when

cells were complemented with the WT-TFEB plasmid (Figure 7F). Treatment of
370 infected shCTRL and shTFEB cells with the mitochondria-targeted ROS-scavenger, Mitotempo, attenuated the expression of inflammatory cytokines (Figure 7G), which further confirmed that mtROS was a key mediator of inflammation in the absence of TFEB. We next asked if silencing *LONP1* could reduce inflammation during infection and found that IL-6 production was dampened upon *S.* Typhimurium infection by
375 silencing *LONP1* (Figure 7H) or pharmacologically inhibiting LONP1 (Figure S7F), or upon inhibition of complex I using Rotenone (Figure S7G). Consistently, mtROS production was also dampened upon the loss of *LONP1* (Figure 7H) or its inhibition using CDDO (Figure S7H). These data suggest that loss of TFEB enhances mtROS mediated inflammation upon *S.* Typhimurium infection, which is dependent on LONP1-
380 regulated mitochondrial complex I.

Discussion

The transcriptional role of TFEB in activating several physiological functions and pathologies is well established (Lapierre *et al.*, 2013; Napolitano & Ballabio, 2016);
385 however, to our knowledge a non-nuclear function is unprecedented. Our efforts to understand the cellular defense mechanisms targeted by *S.* Typhimurium led us to identify a novel mitochondrial role for TFEB. We have deciphered mTOR-dependent translocation of TFEB into mitochondria where it regulates mitochondrial complex I by forming a complex with LONP1 (Figure 7G).
390 Starvation and lysosome storage disorder induced TFEB relocation are the most widely studied, but other stimuli such as lipopolysaccharide (LPS) and pathogens like *Staphylococcus aureus* have also been shown to promote TFEB nuclear translocation. We show that *S.* Typhimurium prevents TFEB translocation into the nucleus,

consistent with our previous report that *S.* Typhimurium infection only transiently activates autophagy (Ganesan *et al.*, 2017). During *S. aureus* infection, nuclear localization of TFEB is associated with the transcription of pro-inflammatory cytokines (Visvikis *et al.*, 2014). Though *S.* Typhimurium infection prevented TFEB nuclear translocation, TFEB depletion further increased the secretion of pro-inflammatory cytokines underscoring a non-nuclear function of TFEB and inflammation regulated by other factors independent of TFEB.

Through multiple lines of evidence, we have demonstrated that TFEB localizes in mitochondria and critically regulates mitochondrial function, with broad implications for its role in health and disease. We show that TFEB resides mostly in the mitochondrial matrix through immunoprecipitation-MS proteomics, confocal microscopy, STED microscopy, immunogold labeling EM, mitochondrial fractionation, mitochondrial pulldown, protease protection and cell free import assays. Additionally, we were able to show the presence of the endogenous TFEB in different cell lines (HeLa and HEK), and in primary human monocyte derived macrophages.

Other transcription factors such as p53, STAT3, and NF-κB that regulate inflammatory pathways also localize in the mitochondria (Szczepanek *et al*, 2012), and in some cases bind to the mtDNA and induce mitochondrial gene transcription. More recently, it has also been reported that the Microphthalmia Transcription Factor (MITF) which also belongs to the same family of basic helix-loop-helix leucine zipper transcription factors as TFEB, interacts with Pyruvate Dehydrogenase (PDH) in the mitochondria modulating its activity, which is crucial in the regulation of the development and the activity of the mast cells (Sharkia *et al*, 2017).

The majority of the proteins destined to the mitochondrial matrix are synthesized with amino terminal pre-sequence or matrix-targeting sequence (MTS) (Backes &

Herrmann, 2017). MTS is recognized by the receptors TOMM20/TOMM22 and
420 TOMM70 on the mitochondrial surface, however, they are cleaved in the mitochondrial matrix to form mature proteins that fold into their native structure (Backes & Herrmann, 2017). We predicted an MTS sequence within TFEB, which was apparently not necessary for its mitochondrial translocation. However, other mechanisms that involve recognition of a specific consensus motif in the translocase of TOMM20 also enable
425 mitochondrial translocation of proteins (Endo & Kohda, 2002; Ramage *et al*, 1993). In this study we identified a specific TOMM20 binding consensus motif in TFEB represented as ϕχχϕϕ (where ϕ is a hydrophobic amino acid and χ is any amino acid) (Saitoh *et al*, 2007). Mutating one amino acid in this binding motif (V to K-30 aa) was sufficient to prevent TFEB mitochondrial translocation. Hence, we termed this motif as
430 mitochondria localization sequence (MLS). The mechanism of translocation was further confirmed by co-immunoprecipitation of both endogenous and ectopically expressed WT-TFEB, with the outer mitochondrial membrane TOMM20, which was lost in the MLS-TFEB mutant, further indicating that the MLS is responsible for its mitochondrial translocation. One of the major hurdles in investigating the mitochondria-
435 centered role of nuclear transcription factors is the dissection of their mitochondrial and nuclear function. Identification of the MLS enabled us to overcome this issue and discern that the nuclear transcriptional function of TFEB was unperturbed even when the MLS was mutated. Interestingly, this motif is conserved in higher mammals, but *zebrafish* and *C. elegans* lack this motif, suggesting a derived function arising late in
440 evolution. Consistently, the TFEB orthologue HLH-30 in *C. elegans* does not translocate to the mitochondria.

The shuttling of transcription factors between the nucleus and mitochondria is regulated by different stress factors (Sepuri *et al*, 2017). Inhibiting mTORC1 upon

starvation or using torin-1 results in the nuclear relocation of dephosphorylated TFEB
445 (Settembre *et al.*, 2012a). We also observed that the interaction of TFEB with mitochondrial proteins is stress-dependent, as it is differentially modulated upon *S.* Typhimurium infection and mTOR-inhibition. TFEB subcellular localization is mediated by mTOR-dependent phosphorylation of the serine residues Ser122, Ser142, and Ser211 (Settembre & Ballabio, 2011). Our mass spectrometry analysis
450 revealed that the mitochondrial TFEB is also not phosphorylated. These findings corroborate with our interactomics data, which shows a positive interaction of TFEB with mitochondrial proteins in torin-1-treated cells. Additionally, *S.* Typhimurium prevented TFEB mitochondrial translocation at later time point of infection, which correlates with our previous findings (Ganesan *et al.*, 2017; Tattoli *et al*, 2012) that it
455 activates mTOR and thereby inhibits autophagy.

Recent reports have indicated that loss of TFEB results in the accumulation of dysfunctional mitochondria (Mansueto *et al.*, 2017). Consistently, TFEB depleted cells, show altered mitochondrial morphology (more perinuclear mitochondria compared to control cells), and activity. ATP-linked respiration and Maximal respiration were
460 increased in TFEB depleted cells, which could be restored when the cells were complemented with the WT-TFEB but, could not be rescued with the MLS-TFEB (mutant of TFEB unable to translocate into mitochondria), or with TFEB exclusively localized in cytoplasm or nucleus, which further demonstrated the mitochondria specific function of TFEB in the regulation of OXPHOS. This finding was further
465 supported by mass spectrometry-based quantification of mitochondrial proteins from TFEB-depleted cells, which indicated enhanced expression of complex I subunits of the mitochondrial electron transport chain (ETC). Moreover, complex I activity in TFEB-depleted cells was also increased, suggesting a role for TFEB in regulating complex I

function. We specifically found that the NDUFA8 and NDUFB10 subunits were
470 increased in TFEB-depleted cells. Overexpression of TFEB increases complex I-IV activity in PGC1α KO muscle cells and the subunits of complex I (NDUFA9), complex II (SDHA), and complex IV (COX5a) (Mansueto *et al.*, 2017). The discrepancies between studies could be attributed to the cell types studied and the subunits analyzed. Moreover, complementation of TFEB-depleted cells with the WT-TFEB, restored the
475 elevated levels of NDUFA8 and NDUFB10. However, restoration was not possible when cells were complemented with MLS-TFEB, indicating the regulation of these two complex I subunits by mitochondrial TFEB. Thus, our investigations suggest that TFEB-regulated mitochondrial function is not solely dependent on its transcriptional activity, but also linked to a mitochondria-specific function.

480 LONP1 is a nuclear-encoded mitochondrial serine protease that regulates proteostasis in mitochondria, mtDNA replication and oxidative phosphorylation (Bota & Davies, 2016; Quiros *et al*, 2015). LONP1 over-expression results in impaired complex I assembly in melanoma cells, up-regulation of NDUFB6,8,10 and 11, and down-regulation of NDUFV1, NDUFV2, NDUFS3 and NDUFS7 (Pinti *et al.*, 2016;
485 Quiros *et al*, 2014). These changes lead to altered respiration and up-regulated glycolysis (Quiros *et al.*, 2014). Consistently, we found that knocking down LONP1 in TFEB-depleted background reduced NDUFA8 and NDUFB10 but restored the oxygen consumption rate and ATP-linked respiration to baseline levels. Interestingly, LONP1 also co-immunoprecipitated with TFEB confirmed by mass spectrometry
490 (Supplemental Table1) and immunoblotting which imply that they co-regulate complex I function. These findings suggest that TFEB and LONP1 can regulate either the assembly or turnover of Complex I which will be very interesting to explore in the future.

Increased LONP1 expression reduces the use of NADH equivalents and the respiration through complex I (Santidrian *et al*, 2013). As a consequence, reactive oxygen species produced by complex I activate p38, JNK, ERK1,2 and Ras-ERK signaling, which favors inflammation (Benhar *et al*, 2001). Correspondingly, inhibition of LONP1 dampened *S.* Typhimurium-induced inflammatory cytokines. LONP1 inhibitor CDDO has shown promising anti-cancer activity and it is compelling to speculate that the outcome could be influenced by the mitochondrial function of TFEB. Dysfunctions in complex I and ETC not only impact energy metabolism, but are also associated with neurodegenerative diseases (Wallace, 2010), cancer-progression (Urra *et al*, 2017), and inflammation(Yu *et al*, 2015). Consistent, with previous reports (Garaude *et al*, 2016), inhibition of complex I resulted in decreased *S.* Typhimurium-induced IL-6. Therefore, we propose that modulating the mitochondrial localization of TFEB has the potential to mitigate complex I associated diseases. mTOR-dependent mitochondrial translocation of TFEB suggests that the efficacy of mTOR inhibitors used in the clinic as immunosuppressant and in cancer therapy is possibly dependent on the mitochondrial activity of TFEB. In the future, it will be fascinating to extend the physiological relevance of the mitochondria-intrinsic function of TFEB in animal models.

Author Contributions: N.R. and C.C. conceived the project. N.R., A.A, S.P and C.C designed experiments and wrote the manuscript. C.C. carried out most of the experiments. H.N. performed and analyzed all the proteomic experiments. M.P performed protein interaction studies. J.F., R.G., S.C and S.G. contributed to the development and analysis of experiments. D.T. edited the manuscript. R.L. performed the experiments in *C. elegans* and designed the graphical abstract. R.R. and P.L. gave technical assistance in the biochemical experiments performed in mitochondria. **Competing interests:** the authors declare no competing financial interests.

Additional information: The mass spectrometry proteomics data have been deposited to the ProteomeXchange Consortium via the PRIDE partner repository with the dataset identifier PXD013758.

Acknowledgments:

We thank the Robinson laboratory members for helpful discussions; Dr. Christian Jüngst, Dr. Astrid Schauss and Ms Beatrix Martiny from the Cluster of Excellence in Cellular Stress Responses in Aging-associated Diseases (CECAD) Imaging Facility, University of Cologne, for assistance with electron microscopy and confocal microscopy; Prof. Thomas Langer (MPI-AGE) for the helpful discussions on mitochondrial experiments; Dr. Oleg Krut and Mr. Paul Moretti for their help in constructing plasmids. Zhara Hejazi for technical support; Dr. Tom MacVicar for assistance with the import assay; Pablo Rivera for the assistance with Sea horse and antibody supply. Dr. Rebecca George Tharyan for scientific discussion. This work was funded by Deutsche Forschungsgemeinschaft through CECAD and SFB670 (to N.R.), the Max Planck Society (to A.A.); the Cologne Graduate School of Ageing Research (to C.C. and R.L.); DZIF (German Center of Infection Research) (to J.F.).

540 **References**

Backes S, Herrmann JM (2017) Protein Translocation into the Intermembrane Space and Matrix of Mitochondria: Mechanisms and Driving Forces. *Frontiers in molecular biosciences* 4: 83

Benhar M, Dalyot I, Engelberg D, Levitzki A (2001) Enhanced ROS production in oncogenically
545 transformed cells potentiates c-Jun N-terminal kinase and p38 mitogen-activated protein kinase activation and sensitization to genotoxic stress. *Molecular and cellular biology* 21: 6913-6926

Bohovych I, Chan SS, Khalimonchuk O (2015) Mitochondrial protein quality control: the mechanisms guarding mitochondrial health. *Antioxid Redox Signal* 22: 977-994

550 Bota DA, Davies KJ (2016) Mitochondrial Lon protease in human disease and aging: Including an etiologic classification of Lon-related diseases and disorders. *Free radical biology & medicine* 100: 188-198

Brady OA, Martina JA, Puertollano R (2018) Emerging roles for TFEB in the immune response and inflammation. *Autophagy* 14: 181-189

555 Cox J, Mann M (2008) MaxQuant enables high peptide identification rates, individualized p.p.b.-range mass accuracies and proteome-wide protein quantification. *Nat Biotechnol* 26: 1367-1372

Cox J, Neuhauser N, Michalski A, Scheltema RA, Olsen JV, Mann M (2011) Andromeda: a peptide search engine integrated into the MaxQuant environment. *J Proteome Res* 10: 1794-
560 1805

Endo T, Kohda D (2002) Functions of outer membrane receptors in mitochondrial protein import. *Biochim Biophys Acta* 1592: 3-14

Ganesan R, Hos NJ, Gutierrez S, Fischer J, Stepek JM, Daglidu E, Kronke M, Robinson N (2017) Salmonella Typhimurium disrupts Sirt1/AMPK checkpoint control of mTOR to impair
565 autophagy. *PLoS pathogens* 13: e1006227

Garaude J, Acin-Perez R, Martinez-Cano S, Enamorado M, Ugolini M, Nistal-Villan E, Hervas-Stubbs S, Pelegrin P, Sander LE, Enriquez JA *et al* (2016) Mitochondrial respiratory-chain adaptations in macrophages contribute to antibacterial host defense. *Nat Immunol* 17: 1037-1045

570 Hos NJ, Ganesan R, Gutierrez S, Hos D, Klimek J, Abdullah Z, Kronke M, Robinson N (2017) Type I interferon enhances necroptosis of Salmonella Typhimurium-infected macrophages by impairing antioxidative stress responses. *J Cell Biol* 216: 4107-4121

Irazoqui JE (2020) Key Roles of MiT Transcription Factors in Innate Immunity and Inflammation. *Trends in Immunology* 41: 157-171

575 Lapierre LR, De Magalhaes Filho CD, McQuary PR, Chu CC, Visvikis O, Chang JT, Gelino S, Ong B, Davis AE, Irazoqui JE *et al* (2013) The TFEB orthologue HLH-30 regulates autophagy and modulates longevity in Caenorhabditis elegans. *Nat Commun* 4: 2267

Mansueto G, Armani A, Viscomi C, D'Orsi L, De Cegli R, Polishchuk EV, Lamperti C, Di Meo I, Romanello V, Marchet S *et al* (2017) Transcription Factor EB Controls Metabolic Flexibility
580 during Exercise. *Cell Metab* 25: 182-196

Martina JA, Chen Y, Gucek M, Puertollano R (2012) MTORC1 functions as a transcriptional regulator of autophagy by preventing nuclear transport of TFEB. *Autophagy* 8: 903-914

Naik E, Dixit VM (2011) Mitochondrial reactive oxygen species drive proinflammatory cytokine production. *J Exp Med* 208: 417-420

585 Napolitano G, Ballabio A (2016) TFEB at a glance. *J Cell Sci* 129: 2475-2481

Napolitano G, Esposito A, Choi H, Matarese M, Benedetti V, Di Malta C, Monfregola J, Medina DL, Lippincott-Schwartz J, Ballabio A (2018) mTOR-dependent phosphorylation controls TFEB nuclear export. *Nat Commun* 9: 3312
Nezich CL, Wang C, Fogel AI, Youle RJ (2015) MiT/TFE transcription factors are activated during mitophagy downstream of Parkin and Atg5. *Journal of Cell Biology* 210: 435-450
Nolte H, MacVicar TD, Tellkamp F, Kruger M (2018) Instant Clue: A Software Suite for Interactive Data Visualization and Analysis. *Sci Rep* 8: 12648
Ouimet M, Koster S, Sakowski E, Ramkhelawon B, Van Solingen C, Oldebeken S, Karunakaran D, Portal-Celhay C, Sheedy FJ, Ray TD *et al* (2016) Mycobacterium tuberculosis induces the miR-33 locus to reprogram autophagy and host lipid metabolism. *Nature immunology* 17: 677-686
Palmieri M, Pal R, Nelvagal HR, Lotfi P, Stinnett GR, Seymour ML, Chaudhury A, Bajaj L, Bondar VV, Bremner L *et al* (2017) mTORC1-independent TFEB activation via Akt inhibition promotes cellular clearance in neurodegenerative storage diseases. *Nature communications* 8: 14338
Park K, Lim H, Kim J, Hwang Y, Lee YS, Bae SH, Kim H, Kim H, Kang S-W, Kim JY *et al* (2022) Lysosomal Ca2+-mediated TFEB activation modulates mitophagy and functional adaptation of pancreatic β-cells to metabolic stress. *Nature communications* 13
Pastore N, Brady OA, Diab HI, Martina JA, Sun L, Huynh T, Lim JA, Zare H, Raben N, Ballabio A *et al* (2016) TFEB and TFE3 cooperate in the regulation of the innate immune response in activated macrophages. *Autophagy* 12: 1240-1258
Pinti M, Gibellini L, Nasi M, De Biasi S, Bortolotti CA, Iannone A, Cossarizza A (2016) Emerging role of Lon protease as a master regulator of mitochondrial functions. *Biochim Biophys Acta* 1857: 1300-1306
Quiros PM, Espanol Y, Acin-Perez R, Rodriguez F, Barcena C, Watanabe K, Calvo E, Loureiro M, Fernandez-Garcia MS, Fueyo A *et al* (2014) ATP-dependent Lon protease controls tumor bioenergetics by reprogramming mitochondrial activity. *Cell Rep* 8: 542-556
Quiros PM, Langer T, Lopez-Otin C (2015) New roles for mitochondrial proteases in health, ageing and disease. *Nature reviews Molecular cell biology* 16: 345-359
Ramage L, Junne T, Hahne K, Lithgow T, Schatz G (1993) Functional cooperation of mitochondrial protein import receptors in yeast. *Embo j* 12: 4115-4123
Roczniak-Ferguson A, Petit CS, Froehlich F, Qian S, Ky J, Angarola B, Walther TC, Ferguson SM (2012) The transcription factor TFEB links mTORC1 signaling to transcriptional control of lysosome homeostasis. *Sci Signal* 5: ra42
Saitoh T, Igura M, Obita T, Ose T, Kojima R, Maenaka K, Endo T, Kohda D (2007) Tom20 recognizes mitochondrial presequences through dynamic equilibrium among multiple bound states. *The EMBO journal* 26: 4777-4787
Santidrian AF, Matsuno-Yagi A, Ritland M, Seo BB, LeBoeuf SE, Gay LJ, Yagi T, Felding-Habermann B (2013) Mitochondrial complex I activity and NAD+/NADH balance regulate breast cancer progression. *The Journal of clinical investigation* 123: 1068-1081
Schuster E-M, Epple MW, Glaser KM, Mihlan M, Lucht K, Zimmermann JA, Bremser A, Polyzou A, Obier N, Cabezas-Wallscheid N *et al* (2022) TFEB induces mitochondrial itaconate synthesis to suppress bacterial growth in macrophages. *Nature Metabolism* 4: 856-866
Sepuri NBV, Tammineni P, Mohammed F, Paripati A (2017) Nuclear Transcription Factors in the Mitochondria: A New Paradigm in Fine-Tuning Mitochondrial Metabolism. *Handb Exp Pharmacol* 240: 3-20
Settembre C, Ballabio A (2011) TFEB regulates autophagy: an integrated coordination of cellular degradation and recycling processes. *Autophagy* 7: 1379-1381

Settembre C, De Cegli R, Mansueto G, Saha PK, Vetrini F, Visvikis O, Huynh T, Carissimo A, Palmer D, Klisch TJ (2013) TFEB controls cellular lipid metabolism through a starvation-induced autoregulatory loop. *Nature cell biology* 15: 647-658

Settembre C, Di Malta C, Polito VA, Arencibia MG, Vetrini F, Erdin S, Erdin SU, Huynh T, Medina D, Colella P (2011a) TFEB links autophagy to lysosomal biogenesis. *Science (New York, NY)* 332: 1429-1433

Settembre C, Di Malta C, Polito VA, Garcia Arencibia M, Vetrini F, Erdin S, Erdin SU, Huynh T, Medina D, Colella P *et al* (2011b) TFEB links autophagy to lysosomal biogenesis. *Science* 332: 1429-1433

Settembre C, Zoncu R, Medina DL, Vetrini F, Erdin S, Erdin S, Huynh T, Ferron M, Karsenty G, Vellard MC *et al* (2012a) A lysosome-to-nucleus signalling mechanism senses and regulates the lysosome via mTOR and TFEB. *Embo j* 31: 1095-1108

Settembre C, Zoncu R, Medina DL, Vetrini F, Erdin S, Erdin S, Huynh T, Ferron M, Karsenty G, Vellard MC *et al* (2012b) A lysosome-to-nucleus signalling mechanism senses and regulates the lysosome via mTOR and TFEB. *The EMBO Journal* 31: 1095-1108

Sharkia I, Hadad Erlich T, Landolina N, Assayag M, Motzik A, Rachmin I, Kay G, Porat Z, Tshori S, Berkman N *et al* (2017) Pyruvate dehydrogenase has a major role in mast cell function, and its activity is regulated by mitochondrial microphthalmia transcription factor. *J Allergy Clin Immunol* 140: 204-214 e208

Szczepanek K, Lesnefsky EJ, Larner AC (2012) Multi-tasking: nuclear transcription factors with novel roles in the mitochondria. *Trends Cell Biol* 22: 429-437

Tattoli I, Sorbara MT, Vuckovic D, Ling A, Soares F, Carneiro LA, Yang C, Emili A, Philpott DJ, Girardin SE (2012) Amino acid starvation induced by invasive bacterial pathogens triggers an innate host defense program. *Cell Host Microbe* 11: 563-575

Unuma K, Aki T, Funakoshi T, Hashimoto K, Uemura K (2015) Extrusion of mitochondrial contents from lipopolysaccharide-stimulated cells: Involvement of autophagy. *Autophagy* 11: 1520-1536

Urra FA, Munoz F, Lovy A, Cardenas C (2017) The Mitochondrial Complex(I)ty of Cancer. *Frontiers in oncology* 7: 118

Visvikis O, Ihuegbu N, Labed SA, Luhachack LG, Alves AF, Wollenberg AC, Stuart LM, Stormo GD, Irazoqui JE (2014) Innate host defense requires TFEB-mediated transcription of cytoprotective and antimicrobial genes. *Immunity* 40: 896-909

Wallace DC (2010) Mitochondrial DNA mutations in disease and aging. *Environ Mol Mutagen* 51: 440-450

Wirth C, Brandt U, Hunte C, Zickermann V (2016) Structure and function of mitochondrial complex I. *Biochim Biophys Acta* 1857: 902-914

Xu Y, Ren J, He X, Chen H, Wei T, Feng W (2019) YWHA/14-3-3 proteins recognize phosphorylated TFEB by a noncanonical mode for controlling TFEB cytoplasmic localization. *Autophagy* 15: 1017-1030

Yu AK, Song L, Murray KD, van der List D, Sun C, Shen Y, Xia Z, Cortopassi GA (2015) Mitochondrial complex I deficiency leads to inflammation and retinal ganglion cell death in the Ndufs4 mouse. *Hum Mol Genet* 24: 2848-2860

Zhang X, Cheng X, Yu L, Yang J, Calvo R, Patnaik S, Hu X, Gao Q, Yang M, Lawas M *et al* (2016) MCOLN1 is a ROS sensor in lysosomes that regulates autophagy. *Nature communications* 7: 12109

Figure Legends

Figure 1. TFEB localizes to mitochondria. (A) Hierarchical clustering using Euclidean distance and complete method for row dendrogram calculations representing the core TFEB interactome. Shown are individual replicates of the WT-TFEB pull down in untreated conditions (UT), upon torin-1 treatment and upon
685 *S.* Typhimurium infection (*S*T). The CTRL is represented by a pull down of another non-specific-FLAG tagged protein used as negative control for the interactions. Log2 LFQ intensities were Z-Score normalized. 14-3-3 proteins as well as the bait TFEB are highlighted in bold font. **(B)** Countplot indicating cellular localization (based on Gene Ontology cellular component annotations) of identified potential interaction partners.
690 "+" symbol corresponds to a known localization either in mitochondria or nucleus. "-" symbol corresponds to an unknown localization in the same compartments. Points and lines indicate categorical group and the bar graph indicates the number of proteins matching the categorical group. **(C)** Hierarchical clustering of TFEB-interacting mitochondrial proteins. Shown are individual replicates similar to Fig 1A. **(D)** HeLa cells
695 ectopically expressing TOMM20-GFP and nucleus. Scale bar = 10 μM. **(E)** Colocalization of TFEB and TOMM20 from Figure 1D was evaluated in ROIs (25x25 pixels) as described in Methods section. Mander's colocalization coefficients using the calculated thresholds (tM) were determined for the green (tM1) (TOMM20) and the red (tM2) (TFEB) channels. Seven cells per group were analyzed. **(F)** TFEB expression in
700 subcellular fractions from shCTRL and shTFEB cells. LAMINB, TOMM20, and GAPDH served as loading controls for the nucleus, mitochondria, and cytoplasm, respectively. Western blot is representative of two independent experiments showing similar results. **(G)** Quantitation of endogenous TFEB levels in subcellular fractions. **(H)** TFEB expression in 10% of total lysate (positive control) and in highly enriched mitochondria
705 isolated from HEK cells using TOMM22-magnetic beads. TOMM20 was used to

confirm the enrichment of mitochondria. PDI was used to exclude ER contaminations; LAMINB to exclude nuclear contaminations and GAPDH to exclude cytosolic contaminations.

710 **Figure 2. TFEB translocates into the mitochondrial matrix in a membrane-potential-dependent manner. (A)** HeLa cells were stained for mitochondrial DNA (mtDNA) using the fluorescent DNA-specific dye PicoGreen and endogenous TFEB. Arrows indicate co-localization. Scale bar = 10 μM. **(B)** Protease protection assay on purified mitochondria isolated from HeLa cells using 50 μg trypsin in the presence or
715 absence of swelling buffer. Samples were analyzed for the outer mitochondrial membrane (OMM) protein TOMM20, the inner mitochondrial membrane (IMM) protein TIM23, and the mitochondrial matrix (MM) protein SLP2. SLP2 and endogenous TFEB were exposed to trypsin after mitochondria were lysed with Triton X-100. Western blot is representative of two independent experiments showing similar results. **(C)**
720 Densitometric analysis of protein levels in Fig. 2b. Band intensities were normalized to the first lane (untreated mitochondria) of the respective protein. **(D)** Immunogold endogenous-TFEB labelling in mitochondria of HeLa cells. Arrows indicate immunogold particles detected in the nucleus (n), cytosol (c) and mitochondria (m). Scale bar = 200 nm. **(E)** Synthetic dataset of observed gold particles deposited on
725 organelle-based compartments. Gold particles were counted using stereology method, applied on 20 images. G_o values indicate the number of Gold particles observed; G_e values indicate the number of Gold particles expected. **(F)** Import assay performed on isolated mitochondria using in vitro synthesized [^{35}S]WT-TFEB. Samples treated with trypsin were assayed in presence (+) or absence (-) of mitochondrial membrane
730 potential ($\Delta\psi$) at different time points. Mitochondria lysed with Triton X-100 were loaded

as a control. **(G)** Graph represents quantification of the *in vitro* [^{35}S]WT-TFEB import assay shown in Figure 2F. The experiment was performed twice showing similar results.

Figure 3. TFEB import into mitochondria depends on a mitochondria localization
735 **sequence (MLS) and mTOR. (A)** Graphical representation of the WT-TFEB FLAG plasmid and the MLS-TFEB FLAG plasmid showing the predicted MLS domain. **(B)** Analysis of subcellular fractions isolated from cells expressing FLAG, WT-TFEB- FLAG or MLS-TFEB-FLAG. LAMINB, TOMM20, and GAPDH served as controls for nucleus, mitochondria, and cytoplasm, respectively. Western blot is representative of three
740 independent experiments showing similar results. **(C)** Import assay using in vitro synthesized [^{35}S]MLS-TFEB performed on isolated mitochondria. Samples were treated with trypsin and assay was performed in presence (+) or absence (-) of mitochondrial membrane potential ($\Delta\psi$) at different time points. Mitochondria lysed with Triton X-100 were loaded as control. **(D)** Conservation of the MLS sequence (red). **(E)**
745 mRNA levels of TFEB target genes (relative to HPRT) from shCTRL and shTFEB transfected with FLAG, WT-TFEB- FLAG or MLS-TFEB-FLAG. Shown are mean ± SEM, n=3 biological replicates. **(F and G)** Endogenous TFEB in subcellular fractions isolated from HeLa cells in untreated conditions (UT) and upon 1 h torin-1 treatment. LAMIN B, TOMM20, and GAPDH served as controls for nucleus, mitochondria, and
750 cytoplasm, respectively. Western blot is representative of three independent experiments showing similar results. **(H)** TFEB structure showing phosphorylation sites in untreated and torin-1-treated cells identified and quantified by LC-MS/MS. Colors indicate intensities in the cytosol (C) or mitochondria (M). **(I)** Endogenous TFEB was immunoprecipitated (IP) from untreated and torin-1 treated HeLa cells and
755 immunoblotted (IB) for TOMM20 and TFEB; Isotype specific IgG was used as negative

control. The immunoprecipitations were performed twice independently showing similar results.

Figure 4. Loss of TFEB dysregulates mitochondrial architecture and function.
760 **(A)** TOMM20 and nucleus staining in shCTRL or shTFEB cells. Scale bar = 10 μm. The boundaries of the cell are shown with a marking. Phase contrast images of the two cell lines are also shown to compare the size of the cells. **(B)** TOMM20 and nucleus staining in shTFEB cells transfected with FLAG, WT-TFEB- FLAG or MLS-TFEB-FLAG. Scale bar= 10 μm. **(C)** OXPHOS profile normalized to Basal respiration
765 of shCTRL and shTFEB cells transfected with empty FLAG, WT-TFEB and MLS-TFEB plasmids. **(D)** Basal, ATP-linked respiration and Maximal respiration normalized to Basal respiration in shCTRL and shTFEB cells transfected with FLAG, WT-TFEB-FLAG or MLS-TFEB-FLAG. Shown are mean ± SEM, n=3 biological replicates.

770 **Figure 5. Mitochondrial complex I is altered in TFEB-depleted cells. (A)** Schematic representation of the respiratory chain complex I. Colors indicate the log2 fold change of shTFEB cells compared to control cells. **(B)** Blue Native Gel Electrophoresis showing complex I assembly in mitochondria enriched from shCTRL and shTFEB cells. Complex I assembly is representative of three independent experiments showing
775 similar results. SLP2 was used as loading control. **(C)** In-gel complex I activity after incubation with NADH and NBT in mitochondria enriched from shCTRL and shTFEB cells. Numbers represent the intensity of the bands quantified. Complex I activity is representative of two independent experiments showing similar results. **(D)** TFEB, NDUFS5, NDUFA8, NDUFB10, NDUFA9, and GAPDH expression in shCTRL and

780 shTFEB. Western blot is representative of three independent experiments showing similar results. **(E)** Mean densitometric analysis of the immunoblot shown in Fig. 5D. **(F)** NDUBFA8, NDUFB10, TFEB, and GADPH expression in shCTRL and shTFEB transfected with FLAG, WT-TFEB- FLAG or MLS-TFEB-FLAG. Western blot is representative of three independent experiments showing similar results. **(G)** Mean
785 densitometric analysis of the immunoblot shown in Figure 5F.

Figure 6. TFEB and LONP1 co-regulate complex I. (A) TFEB, LONP1, NDUFA8, NDUFB10, and GAPDH expression in HeLa cells transfected with control siRNA (siCTRL), siRNA against LONP1 (siLONP1), TFEB specific siRNA (siTFEB) and siRNA against both LONP1 and TFEB. Western blot is representative of three
790 independent experiments showing similar results. **(B)** Mean densitometric analysis of the immunoblot from Fig. 6A. Shown are mean ± SEM. **(C)** LONP1, TFEB, NDUFA8, NDUFB10, NDUFS5, NDUFA9 and GAPDH protein expression in shCTRL and shTFEB cells transfected with siCTRL and siLONP1. Western blot is representative of three independent experiments showing similar results. **(D)** Relative mRNA expression
795 of LONP1 and TFEB (relative to RPL13A) in HeLa cells transfected with siCTRL and siLONP1. Shown are mean ± SEM, n=6 biological replicates. **(E)** OXPHOS profile of shCTRL and shTFEB cells transfected with siCTRL and siLONP1. **(F)** ATP-linked respiration and Maximal respiration rates normalized to Basal respiration in shCTRL and shTFEB cells transfected with siCTRL or siLONP1. Shown are mean ± SEM, n=3
800 technical replicates. The data is representative of two independent experiments showing similar results. **(G)** Endogenous TFEB was immunoprecipitated and immunoblotted for LONP1 and TFEB in HeLa cells. Western blot is representative of two independent experiments showing similar results. IgG was used as negative

control. **(H)** TFEB-Flag was pulled down from cells transfected with Empty vector (EV), LONP1-HA, TFEB-FLAG and TFEB-FLAG + LONP1-HA and immunoblotted for LONP1-HA and TFEB-FLAG to confirm TFEB-LONP1 interaction. EV was used as a negative control. Quantifications of the immunoblot are also shown. The experiment was performed in triplicate showing similar results. **(I)** LONP1 was purified and incubated with control beads as negative control and with TFEB- FLAG-tagged beads. The experiment was performed in duplicate showing similar results.

Figure 7. Mitochondrial TFEB regulates inflammation. (A) Endogenous TFEB subcellular localization upon 24 h of *S.* Typhimurium infection (MOI 100) in HeLa cells. LAMINB, TOMM20, and GAPDH served as controls for nucleus, mitochondria, and cytosol, respectively. Western blot is representative of three independent experiments showing similar results. **(B)** Densitometric quantitation of immunoblots depicting the subcellular endogenous TFEB localization in uninfected (UI) and *S.* Typhimurium-infected (MOI=100) cells from Figure 7A. **(C)** IL-6 and **(D)** IL-8 in the supernatants of 24 h *S.* Typhimurium-infected shCTRL and shTFEB cells. Shown are mean ± SEM, n=3 biological replicates. **(E)** IL-6 in supernatants of shCTRL and shTFEB cells transfected with FLAG, WT-TFEB-FLAG or MLS-TFEB-FLAG plasmids and infected for 24 h with *S.* Typhimurium (MOI 100). Shown are mean ± SEM, n=3 biological replicates. **(F)** Flow cytometric analysis of Mitochondrial ROS (mtROS) production was estimated on MitoSOX-stained shCTRL and shTFEB cells transfected with empty FLAG and WT-TFEB-FLAG and the Mean Fluorescence Intensity (MFI) was plotted; mean ± SEM, n=3 biological replicates. **(G)** IL-6 secretion in supernatants of shCTRL and shTFEB cells infected with *S.* Typhimurium (MOI 100) for 24 h and treated with MitoTempo 2 h prior infection and during infection. Shown are mean ± SEM, n=3

biological replicates with n=2 technical replicates each. **(H)** IL-6 expression in
830 supernatants of shCTRL and shTFEB cells transfected with siCTRL and siLONP1 and infected with *S.* Typhimurium (MOI 100) for 24 h. Shown are mean ± SEM, n=2 technical replicates. The experiment was repeated twice with similar results. **(I)** MitoSOX-based flow cytometric detection of mitochondrial ROS production in shCTRL and shTFEB cells transfected with siCTRL and siLONP1. Shown is the Mean
835 Fluorescence Intensity (MFI). Shown are mean ± SEM, n=3 biological replicates. **(J)** A model showing that *S.* Typhimurium prevents mTOR-dependent mitochondrial translocation where it interacts with LONP1 to co-regulate complex I assembly and function.

840 **Material and methods**

Antibodies, siRNAs and primers.

Antibodies and cell-staining reagents are listed in Supplementary Table 2; siRNAs in Supplementary Table 3, and primers in Supplementary Table 4.

Cell culture and treatments

845 Cells were cultured in the following media: HeLa (ATCC) and HEK293T in Dulbecco´s modified Eagle's medium (DMEM) (11960, Life Technologies) supplemented with 10% fetal bovine serum (FBS) (Biowest, S1810-500) and kept at 37 °C in a humidified 5% CO_2 incubator. Stable TFEB knockdown was achieved by transfecting TFEB-specific shRNA cloned in pRFP-C-RS plasmid (OriGene RNAi, 0513). The same plasmid 850 containing non-specific shRNA was used as a control (OriGene RNAi, 0415). The cells were transfected using Lipofectamine 3000 (L3000008, Thermo Fisher Scientific) and the clones resistant to puromycin (A11138-03, Life Technologies) were selected. All the constructs were transfected using Lipofectamine 3000. siRNA transfections were performed using 50 nM of siRNA using Lipofectamine RNAiMax (13778030, Thermo 855 Fisher Scientific) according to the manufacturer's recommendations. The indicated drugs were directly added in the culture medium: torin-1 (10 μM) (4247/10, R&D and Tocris), Rotenone (500 nM) (ab143145, Abcam) and CDDO (2.5 μM) (Cay81035, Biomol), Mitotempo (10 μM) (Sigma Aldrich, SML0737).

860 **Immunocytochemistry**

For immunofluorescence, cells previously seeded on coverslips were fixed with 4% PFA (28908, Thermo Scientific) for 15 min, washed three times in PBS, permeabilized in 0.3% Triton-100 followed by incubation with Image-iT® R FX (#I36933, Invitrogen) and blocked with 5% BSA. Cells were then incubated overnight at 4 °C with specific 865 primary antibodies. The following day, after washing with 0.03% Triton in PBS, cells were incubated with the relevant secondary antibody for 1 h at RT protected from light. ProLong® Gold antifade DAPI (P36962, Invitrogen) was used for nuclear counterstaining. The slides were imaged using a 63X objective under a confocal microscope (Leica SP8, Leica Microsystems).

870 The MitoTracker deep red (M22426, Thermo Fischer Scientific) staining was performed by incubating the cells with 250 nM of Mitotracker deep red in DMEM for 1

h at 37 °C in a humidified 5% CO2 incubator. Coverslips were extensively washed with PBS, prior to mounting with ProLong® Gold antifade DAPI (P36962, Invitrogen).

875 **mtDNA immunohistochemistry**

Cells previously seeded on coverslips were fixed in 4% PFA in PBS for 10 min at RT, and subsequently permeabilized with 0.1% Triton X-100 in PBS for 5 min at RT. After blocking, cells were incubated overnight at 4°C with the primary antibody against mtDNA (61014, Progen), prepared in 3% BSA in PBS. Cells were then incubated with
880 the secondary goat anti-mouse IgM Alexa594 (Invitrogen, A21044) in 3% BSA in PBS for 2 h at RT. Finally, coverslips were extensively washed with PBS, prior to mounting with ProLong® Gold antifade (P10144, Invitrogen).

Constructs, cloning and mutagenesis

885 For experiments based on the expression of ectopic TFEB, cDNAs were cloned into the p162 vector provided by Dr. Oleg Kurt, to generate N-terminally FLAG-tagged TFEB proteins. The MLS-TFEB mutant was generated using the Quikchange XL site-directed mutagenesis kit (200521, Agilent). The ΔMTS mutant was generated by cloning a truncated sequence of TFEB in the pcDNA 3.1 FLAG backbone (121416, In-
890 fusion HD Cloning). The TFEB mutants TFEB-ΔNLS (cytosolic TFEB) and S142A-S211A (nuclear TFEB) were provided by Dr. Oleg Kurt.

Subcellular fractionation assays

Cellular fractionation to prepare cytosolic, mitochondrial, and nuclear extracts was
895 performed using a kit (ab109179, Abcam), according to manufacturer's instructions. The nuclear fraction was finally sonicated. GAPDH, LAMINB and TOMM20 were used as markers for cytosol, nucleus and mitochondria respectively.

Mitochondria purification using anti-TOM22 microbeads

900 HEK293T cells were harvested and mitochondria were purified using anti-TOMM22 labelled magnetic micro-beads according to the manufacturer's instructions (Miltenyi Biotec 130-094-532). 50 μg of purified mitochondria were subjected to Western blot analysis and 10% of total lysate was loaded as positive control.

905 **Preparation of Human Monocyte Derived Macrophages**

After obtaining written consent from healthy donors, blood samples were obtained from 2 female donors in the age of 20-30. CD-14 positive monocytes were isolated from peripheral blood mononuclear cells (PBMCs) and differentiated with M-CSF for 5 days in RPMI/10% FCS for cell culture ex-vivo experiments.

910

Protection assay

Purified mitochondria were resuspended in the mitochondria isolation buffer (MIB, 200 mM mannitol, 70 mM sucrose, 10 mM HEPES/KOH pH 7.4, 1 mM EDTA) and incubated with 2.5 μg of trypsin for 15 min on ice. The swelling buffer was prepared in 915 order to cause osmotic shock using 50 mM HEPES/KOH pH 7.2, 0.6 M Sorbitol and 80 mM KCl. 1% Triton X-100 was eventually added to permeabilize the mitochondrial membranes and allow the trypsin to reach the mitochondrial matrix. Samples were then subjected to SDS-PAGE and immunoblotting. Anti-TOMM20, TIMM23 and SLP2 (or MRPL12 in HEK293T) antibodies were used to analyze trypsin-mediated 920 degradation of proteins located in the outer mitochondrial membrane (OMM), the inner mitochondrial membrane (IMM), and the mitochondrial matrix (MM), respectively.

***In vitro* import assay**

Purified mitochondria were resuspended in the mitochondria isolation buffer (MIB, 220 925 mM mannitol, 140 mM Sucrose, 10 mM HEPES/KOH pH 7.4, 1 mM EGTA/KOH).

For *in vitro* import assay WT and MLS-TFEB cDNA were cloned into the pGEM-4 vector and transcribed *in vitro* using the TNT Quick coupled translation system (L1170, Promega), by incubating 200 ng of DNA with 7 μL of TNT-T7 reticulocyte lysate mix and 0.5 μL of 35S-labelled methionine (NEG709A500UC, PerkinElmer) for 1 h at 30 930 °C at 600 rpm. Next, the mitochondrial pellets were resuspended into mitochondrial import buffer (500 mM Sucrose, 10 mM MgAc, 160 mM KAc, 20 mM sodium succinate and 40 mM Hepes-KOH pH 7.4, 0.3 M ATP, and 1 M fresh DTT). Then, mitochondria were incubated with the lysate containing TFEB transcribed in vitro and the membrane potential was blocked by adding 1 μL of 20 mM CCCP at different time points. 935 Mitochondria were also treated with Trypsin (T1426, Sigma Aldrich) (25 μg/mL for 10 min) followed by trypsin inhibitor soya bean (Merck, 10109886001) (250 μg/mL for 15 min). 1% Triton X-100 was eventually added to permeabilize the mitochondrial

membranes and allow the trypsin to reach the mitochondrial matrix. The mitochondrial pellet was lysed in denaturing conditions and proteins were detected by autoradiography.

Seahorse XFe96 metabolic flux analysis

Cellular respiration was measured using the Seahorse XFe96 analyzer (Agilent) following manufacturer´s recommended protocols. Briefly, HeLa cells were seeded in a 6 well-plate and transfected with FLAG, WT-TFEB FLAG, MLS-TFEB, NLS-TFEB and NL-TFEB FLAG plasmids, or with siCTRL and siLONP1. After 24 h, cells were seeded in a 96 well-plate and the next day the plates were incubated in 180 μL of assay media at 37 °C in a CO_2 free incubator for 1 h. The plates were assayed on the XFe96 analyzer to calculate the oxygen consumption rate (OCR) over time after sequential addition of different drugs. Their final concentrations in the assay were: Oligomycin (6 μM), FCCP (0,5 μM), Rotenone (0,5 μM), and Antimycin A (0,5 μM).
HEK293T cells, were seeded in a 6 well-plate and transfected with siRNA CTRL and siRNA against TFEB. After 24 h, cells were seeded in a Poly-D-Lysin pre-coated 96 well-plate. Next day, the plates were incubated in 180 μL of assay media at 37°C in a CO_2 free incubator for 1 h. The plates were assayed on the XFe96 analyzer to calculate the oxygen consumption rate (OCR) over time after sequential addition of different drugs. Their final concentrations in the assay were: Oligomycin (6 μM), FCCP (0.3 μM), Rotenone (0.5 μM), and Antimycin A (0.5 μM). After the run, the assay media was removed, and the cells were lysed for analysis. The data were normalized with protein estimated by Bradford assay.

Western blotting

Western blotting was performed on proteins extracted using RIPA buffer containing complete protease and phosphatase inhibitor cocktail. Samples were incubated on ice for 20 min and centrifuged at 13200 rpm for 10 min. BCA was done to quantify the amount of proteins in the lysates. Required samples were mixed 1:1 with 2X sample loading buffer, boiled at 95°C, and resolved by SDS-PAGE. Proteins were then transferred onto a PVDF membrane blocked with 5% milk or BSA and probed with the respective primary antibodies, followed by treatment with an appropriate secondary antibody conjugated to horseradish peroxidase. The blots were developed using an

enhanced chemiluminescence substrate (GE Health sciences) and bands were identified by exposing the membrane on to an X-ray film or imaged using the ChemiDoc Imaging System (Biorad). Densitometric analysis of immunoblots was performed using NIH ImageJ.

975

Salmonella Typhimurium infection

HeLa cells were seeded in tissue culture plates and infected with *S.* Typhimurium (SL1344) (MOI 100). After 30 min, extracellular bacteria were removed and cells were incubated for 2 h in medium containing 50 µg/ml Gentamicin (15750037, Life
980 Technologies). Then, the cells were washed and subsequently cultured in medium containing lower concentration of Gentamicin (10 µg/ml). Cells were collected for analysis at the desired time points.

mtROS detection

985 mtROS was determined with MitoSOX (M36008, Thermo Fisher Scientific) according to the manufacturer's instructions. At the indicated time points, HeLa cells (0.5×10^6 cells/well) were resuspended in 1% (wt/vol) PFA in PBS. For each experiment, 50,000 cells were acquired using a flow cytometer (FACSCanto; Becton Dickinson) and analyzed using FLOWJO software (Tree Star).

990

RNA extraction and quantitative PCR

Total RNA was extracted from cells in QIAzol reagent (79306, Qiagen), using RNeasy kit (74106, Qiagen). RNA was reverse transcribed using the iScript cDNA synthesis kit (1708891, Biorad). The resulting cDNA was quantified by real-time qPCR using the
995 LightCycler 480 SYBR Green Master Mix (4367659, Thermo Fisher Scientific). The relative mRNA levels were calculated using the ΔΔCt method and normalized to Hypoxanthine-Guanine-Phosphoribosyl-Transferase (HPRT) or to Ribosomal Protein L13, (RPL13A) mRNA levels.

1000 **Co-immunoprecipitations**

For endogenous immunoprecipitations, 10^7cells were lysed in cell lysis buffer (98035S, Cell Signaling Technology) containing protease inhibitors (4693159001, Roche) and incubated for 15 min on ice. Immunoprecipitation was performed by incubating 1 mg

of the whole cell lysates (input) with 2 μg of antibody overnight at 4 °C. Isotype specific
1005 rabbit IgG (2729, Cell Signaling Technology) was used as negative control. The following day, protein A sepharose beads (101041, Thermo Fischer Scientific) were added and incubated for 2 h at 4 °C. The immunocomplexes were then washed 3 times with lysis buffer, resuspended in Laemli buffer, and samples were boiled at 95°C for 5 min and processed for immunoblotting.
1010 For the ectopic immunoprecipitations, 10^7 cells overexpressing TFEB- FLAG and LONP1 were lysed in cell lysis buffer (98035S, Cell Signaling Technology) containing protease inhibitors (4693159001, Roche) and incubated for 15 min on ice. Immunoprecipitation was performed by incubating 1 mg of the whole cell lysates (input) with M2 mouse anti-FLAG (F3165, Sigma Aldrich) and 50 μL of microMACS Protein G
1015 magnetic beads (Miltenyi, 130-042-701). Samples were washed with 150 μL 50 mM Tris-HCl pH 7.4, 1% NP-40 and then eluted into Laemli buffer, and samples boiled at 95 °C for 5 min and processed for immunoblotting.

Protein purification and interaction

1020 TFEB-FLAG and LONP1-HA were overexpressed in HEK293T cells and were harvested after 24 h. The pellets were lysed into Lysis buffer (20 mM Tris-HCl pH 7.5, 150 mM NaCl, 1 mM EDTA, 1 mM EGTA, 1% Triton, 2.5 mM sodium pyrophosphate, 1 mM b-glycerophosphate, 1 mM Na3 VO4 and protease inhibitors (4693159001, Roche), incubated for 15 min on ice and centrifuged at 17000 x g for 10 min and
1025 cleared lysates were collected. CTRL vector or TFEB-FLAG lysates were incubated with M2 anti-FLAG agarose beads (A22220, Sigma Aldrich) for 3 min at 4°C on wheel. The beads were then washed 4 times with Buffer A: 50 mM Tris-HCl pH 7.4, 150 mM NaCl, 0.05% Tx100, 10% glycerol, 1 mM EDTA, 2.5 mM sodium pyrophosphate, 1 mM b-glycerophosphate and 1 mM Na3 VO4.
1030 LONP1 lysate was incubated with anti-HA antibody and protein G sepharose beads (20398, Thermo Fischer Scientific) for 30 min at 4 °C on wheel. Beads were washed 4 times with Buffer A and samples were eluted with 1mg/mL of HA-peptide in buffer Aby incubating 30 min at 4 °C on wheel. The CTRL and TFEB-FLAG beads were added to the purified LONP1 and the samples were eluted in Laemli buffer.
1035

Staining in *C. elegans*

The strain used for the mitochondrial staining is *hlh-30(syb809) IV* which has the endogenous *hlh-30* locus tagged with mNeonGreen by CRISPR/Cas9. Synchronized
1040 eggs were incubated on NGM agar plates with *E. coli* strain OP50 containing 500 nM MitoTracker Deep Red FM (Invitrogen M22426) until day 1 adults. The worms were mounted on 5% agarose pads and anesthetized with 20mM levamisole. Pictures were taken with confocal laser scanning microscopy platform Leica TCS SP8.

1045 **Blue native**

For blue native electrophoresis, mitochondria were solubilized in lysis buffer (50 mM NaCl, 10% glycerol, 5 mM 6-aminohexanoic acid, 50 mM imidazole/HCl pH 7.0, 50 mM KP_i buffer pH 7.4) containing 1% (w/v) digitonin for 30 min on ice. Insoluble material was removed by centrifugation and subjected to blue native electrophoresis.

1050

In gel enzymatic activity staining

Purified mitochondria were subjected to blue native electrophoresis and the gels were rinsed briefly in MilliQ water and then equilibrated in reaction buffer (0.1 M Tris-HCl pH 7.4) without substrates for 10 min. The gels were then incubated at room temperature
1055 in fresh buffer plus reagents (0.2 mM NADH and 1 mg/mL NBT) for varying lengths of time until sufficient staining.

Electron microscopy

HeLa cells ($2x10^6$ cells/well) were fixed by immersion in 2% glutaraldehyde, 2.5%
1060 Sucrose, 3 mM $CaCl_2$ and 100 mM HEPES pH 7.4 for 30 min at room temperature and 30 min at 4 °C. After the fixation the cells were washed three times in 0.1 M Sodium Cacodylate buffer. After treatment with Osmium for 1 h on ice, the sections were dehydrated with ethanol and embedded in epoxy resin. The cells were then cut 70 nm thick on a Ultracut from Leica. They were contrasted with 1.5% uranyl acetate for 15
1065 min at 37 °C in the dark, then washed with water 5 times and washed with leadcitrate for 4 min. Finally, the grids were washed 5 times in water and dried on a filter paper. The cells were cut 70 nm thick on an Ultracut from Leica; they were contrasted with 1.5% uranyl acetate for 15 min at 37 °C in the dark, washed with water 5 times and then with leadcitrate 4 min. Finally, the grids were washed 5 times in water and then

1070 dried on a filter paper. Samples were examined with the electron microscope JEOL JEM 2100 plus.

Electron microscopy analysis

To test for preferential labelling of compartments, observed and expected gold
1075 particle distributions are compared by $\chi 2$ analysis. Efficient estimators of gold labelling intensity (relative labelling index (RLI) were calculated to analyze volume-occupying compartments (cytosol, mitochondria and nucleus). Compartment size is estimated by counting chance events after randomly superimposing test lattices of crosses. RLI=1 when there is random labelling and RLI >1 when there is preferential
1080 labelling.

Confocal image analysis

Colocalization was analyzed using Colocalization Analysis plugins (ImageJ software). First, the Colocalization Test plugin with Fay randomization method was performed to
1085 calculate Pearson's correlation coefficient for the two channels in each selected ROI (25 × 25 pixels). This value was compared with what would be expected for random overlap. The observed correlation was considered significant if it was greater than 95% of the correlations between channel 1 and a number of randomized channel 2 images. All ROIs with Pearson's coefficient p value of ≥ 0.95 were further analyzed by the
1090 Colocalization Threshold plugin to calculate thresholded Mander's coefficients [tM1 colocalization value for channel 1 (red); tM2 colocalization value for channel 2 (green or blue)] and to generate scatterplots with linear regression line and thresholds.

ELISA

1095 Cell culture supernatants from HeLa cells (5×10^7 cells/well) were collected 24 h after infection and were kept at –80 °C until assayed for human IL-6 (DY206-05, R&D Systems) and human IL-8 (DY208-05, R&D) according to the manufacturer's instructions.

1100 **Interactome analysis**

TFEB-FLAG IP for immunoblot and mass spectrometry was performed in triplicates for each condition using Anti-FLAG M2 Magnetic Beads, according to the manufacturer's

instructions. Washed beads with enriched proteins were denaturated in 6 M urea/2M thio-urea in 10 mM HEPES buffer. Proteins were reduced by dithiothreitol (DTT) at a final concentration of 10 mM for 30 min at 25°C. Then, proteins were alkylated using Iodacetamide (IAA) at a final concentration of 55 mM in the dark. Proteins were separated by molecular weight on an SDS-PAGE. Gel lanes were cut into 5 equal sized pieces and further cut into 1mm^2 cubes. Gel pieces were washed several times and proteins were digested in-gel using a digestion solution (12 ng/μL Trypsin, 2 ng/μL LysC) was added to cover gel pieces. Generated peptides were extracted by an increasing acetonitrile content. Peptides were concentrated in a SpeedVac to 50 μL. 100 μL 0.1% formic acid was added and samples were desalted using the STAGE tip technique.

Mitochondrial proteome

Mitochondria were isolated in the MIB, and the pellet was resuspended in the following buffer: 50 mM TrisHCl pH 8.0, 2% SDS, 2% CHAPS and 1% NP-40. 500 μg of protein was precipitated by adding 4 volumes of acetone and incubation at -20 °C for at least 15 h. The pellet was washed with 90% acetone and resuspended in 6 M Urea/2M Thio-Urea in 10 mM HEPES. Proteins were reduced using 10 mM Tris (2-carboxyethyl) phosphine (TCEP), alkylated with 20 mM chloroacetamide (CAA) and digested using 1 μL of 0.5 μg/μL of Lys-C at a 1:100 enzyme to substrate ratio to the mixture for 2 h. Then 50 mM Ammonium bicarbonate was used to dilute the Urea concentration to 2 M supplemented with 1 μL of 0.5 μg/μL of Trypsin. Overnight digestion was stopped by Trifluoroacetic acid (TFA) acidification (1% final concentration).

TFEB Phosphorylation Detection

Endogenous TFEB was pulled down in both cell lysates and purified mitochondria. Next, samples were loaded on SDS-PAGE and proteins were separated according to their molecular mass. Gels were stained with InstantBlue for 30 min and gel bands were cut of the matching molecular weight. Proteins were digested in-gel and peptides were desalted prior LC-MS/MS analysis.

Liquid Chromatography and Mass Spectrometry Measurements

1135 Peptides were eluted from home-made StageTips using 60% acetonitrile and 0.1% formic acid and evaporated to complete dryness using a SpeedVac (Eppendorf). Peptides were reconstituted in 2% formic acid and 2% acetonitrile. The LC-MS/MS equipment consisted out of an Easy nLC 1000 (Thermo Fisher Scientific) coupled to a QExactive Plus mass spectrometer via a nano-spray ionization source. Peptides were
1140 separated according to their hydrophobicity using in-house made columns (ReproShell C18, Agilent, 2.7 μm). Column temperature was controlled by an in-house made column oven. Peptides were ionized using a Spray Voltage of 2.4 kV and the mass spectrometer operated in a data-dependent mode (Top10). The MS1 spectra were acquired at a resolution of 70,000 (at 200 m/z) and a maximum injection time of 20 ms.
1145 The mass range was 350-1750 m/z.

The MS2 settings varied depending on the experiment. For whole proteome and interactome (in-solution) analysis, a resolution of 17,500 at 200 m/z and a maximum injection time of 60 ms was used. For detection of phosphorylation sites from pulled down endogenous TFEB, a higher spectra quality was required and a resolution of
1150 30,000 at 200 m/z accompanied with a maximum injection time of 120 ms was utilized.

Raw Data Processing and Analysis

Acquired raw data were analyzed using MaxQuant(Cox & Mann, 2008) and the implemented search engine Andromeda(Cox *et al*, 2011). MS/MS spectra were
1155 correlated to the human Uniprot reference proteome using default settings for mass tolerances. The 'match-between-runs' and MaxLFQ algorithms were enabled using default settings. For detection of phosphorylation sites, a minimum score of 0 was used but MS/MS spectra of detected TFEB sites were inspected manually.

Contaminants, 'only identified by site' and 'reverse' data base hits were removed in
1160 Perseus. LFQ intensities or site intensities were log_2 transformed. Significantly different regulated/enriched proteins were determined by a two-sided t-test using a permutation-based FDR estimation (s0=0.1, number of permutations: 500) for whole proteome and interaction studies. Gene Ontology annotations were added from the Uniprot database. Data were analysed and visualized in Instant Clue(Nolte *et al*, 2018).
1165 Data were uploaded to PRIDE repository and can be found under the following identifier: PXD013758.

Statistical analysis

All the statistical analysis was performed using GraphPad Prism software. Two-tailed
1170 Student's t-test was conducted for most of the data sets unless specified otherwise to determine statistical significance. All data are represented as mean ± SEM as indicated. For all tests, p-values <0.05 was considered statistically significant (*p<0.05; **p<0.01; ***p<0.005).

Fig.1

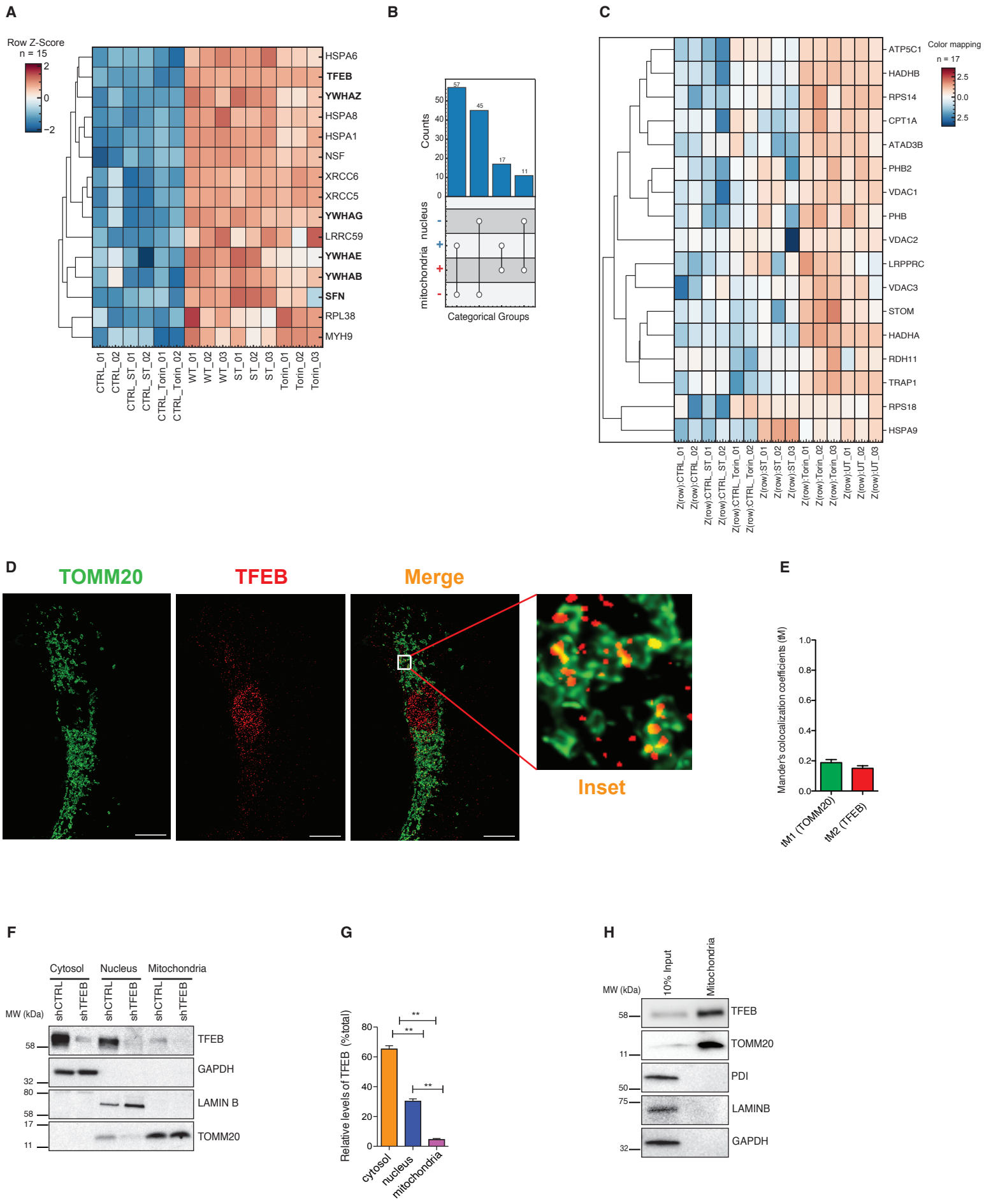
A
Row Z-Score
n = 15
2
0
−2
HSPA6
TFEB
YWHAZ
HSPA8
HSPA1
NSF
XRCC6
XRCC5
YWHAG
LRRC59
YWHAE
YWHAB
SFN
RPL38
MYH9
CTRL_01
CTRL_02
CTRL_ST_01
CTRL_ST_02
CTRL_Torin_01
CTRL_Torin_02
WT_01
WT_02
WT_03
ST_01
ST_02
ST_03
Torin_01
Torin_02
Torin_03
B
Counts
57
45
17
11
mitochondria
nucleus
Categorical Groups
C
Color mapping
n = 17
2.5
0.0
2.5
ATP5C1
HADHB
RPS14
CPT1A
ATAD3B
PHB2
VDAC1
PHB
VDAC2
LRPPRC
VDAC3
STOM
HADHA
RDH11
TRAP1
RPS18
HSPA9
Z(row):CTRL_01
Z(row):CTRL_02
Z(row):CTRL_ST_01
Z(row):CTRL_ST_02
Z(row):CTRL_Torin_01
Z(row):CTRL_Torin_02
Z(row):ST_01
Z(row):ST_02
Z(row):ST_03
Z(row):Torin_01
Z(row):Torin_02
Z(row):Torin_03
Z(row):UT_01
Z(row):UT_02
Z(row):UT_03
D
TOMM20
TFEB
Merge
Inset
E
Mander's colocalization coefficients (tM)
1.0
0.8
0.6
0.4
0.2
0.0
tM1 (TOMM20)
tM2 (TFEB)
F
Cytosol
Nucleus
Mitochondria
shCTRL
shTFEB
shCTRL
shTFEB
shCTRL
shTFEB
MW (kDa)
58
TFEB
GAPDH
32
80
LAMIN B
58
17
TOMM20
11
G
Relative levels of TFEB (%total)
80
60
40
20
0
**
**
**
cytosol
nucleus
mitochondria
H
MW (kDa)
10% Input
Mitochondria
58
TFEB
11
TOMM20
50
PDI
75
LAMINB
32
GAPDH

Fig.2

A

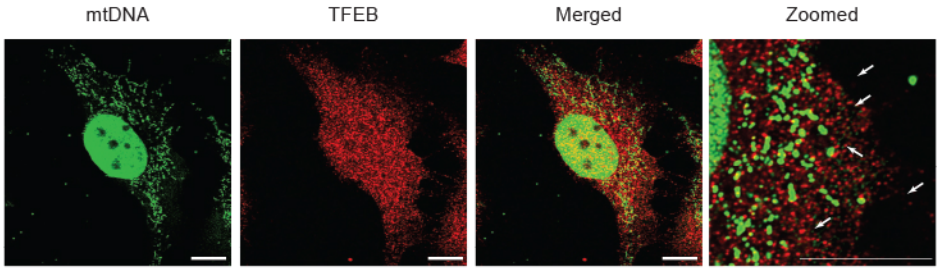

B

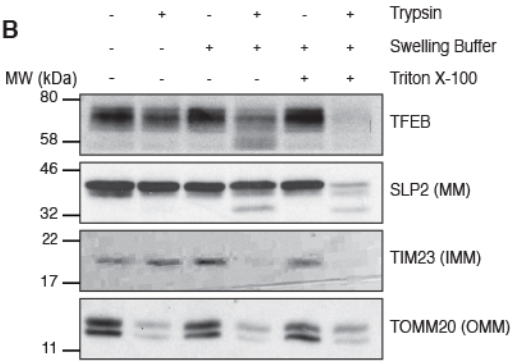

C

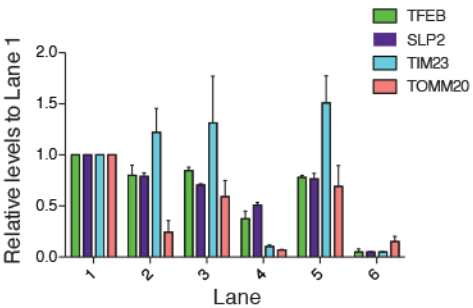

D

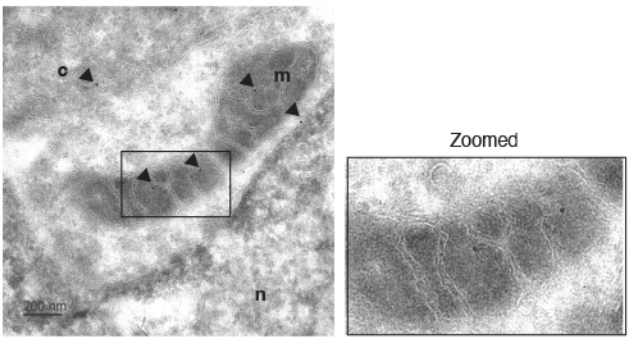

E

Compartment	Gold $count_0$	Gold $count_e$	RLI value	χ^2
Cytosol	98	118.63	0.82	3.58
Nucleus	31	24,46	1.26	1.74
Mitochondria	41	26.90	1.52	7.38
Total	170	170		

F

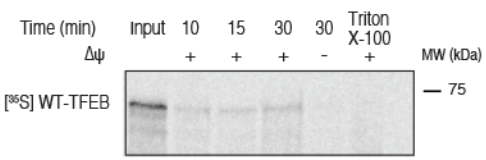

G

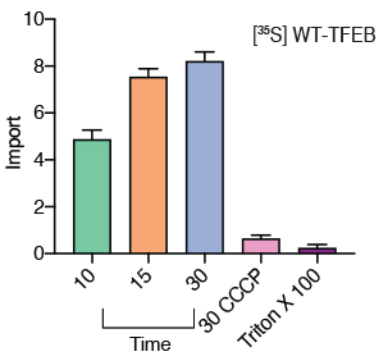

Fig.3

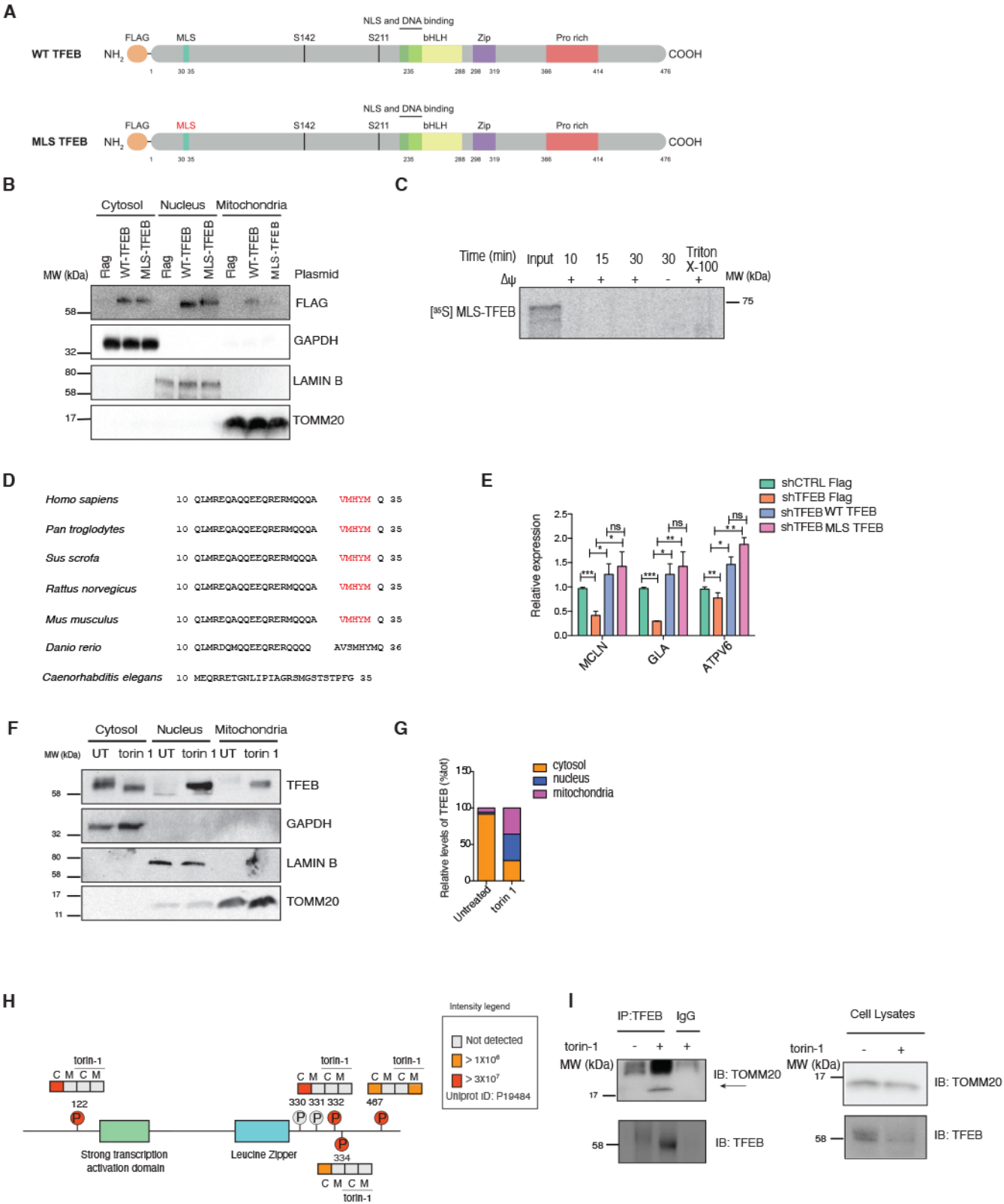
A
WT TFEB
MLS TFEB
NH2
FLAG
MLS
S142
S211
NLS and DNA binding
bHLH
Zip
Pro rich
COOH
B
Cytosol
Nucleus
Mitochondria
Flag
WT-TFEB
MLS-TFEB
MW (kDa)
Plasmid
FLAG
GAPDH
LAMIN B
TOMM20
C
Time (min)
Input
10
15
30
30
Triton X-100
Δψ
[35S] MLS-TFEB
MW (kDa)
75
D
Homo sapiens
Pan troglodytes
Sus scrofa
Rattus norvegicus
Mus musculus
Danio rerio
Caenorhabditis elegans
E
shCTRL Flag
shTFEB Flag
shTFEB WT TFEB
shTFEB MLS TFEB
Relative expression
MCLN
GLA
ATPV6
F
Cytosol
Nucleus
Mitochondria
MW (kDa)
UT
torin 1
TFEB
GAPDH
LAMIN B
TOMM20
G
cytosol
nucleus
mitochondria
Relative levels of TFEB (%tot)
Untreated
torin 1
H
torin-1
Strong transcription activation domain
Leucine Zipper
Intensity legend
Not detected
> 1X10^6
> 3X10^7
Uniprot ID: P19484
I
IP:TFEB
IgG
Cell Lysates
MW (kDa)
IB: TOMM20
IB: TFEB

Fig.4

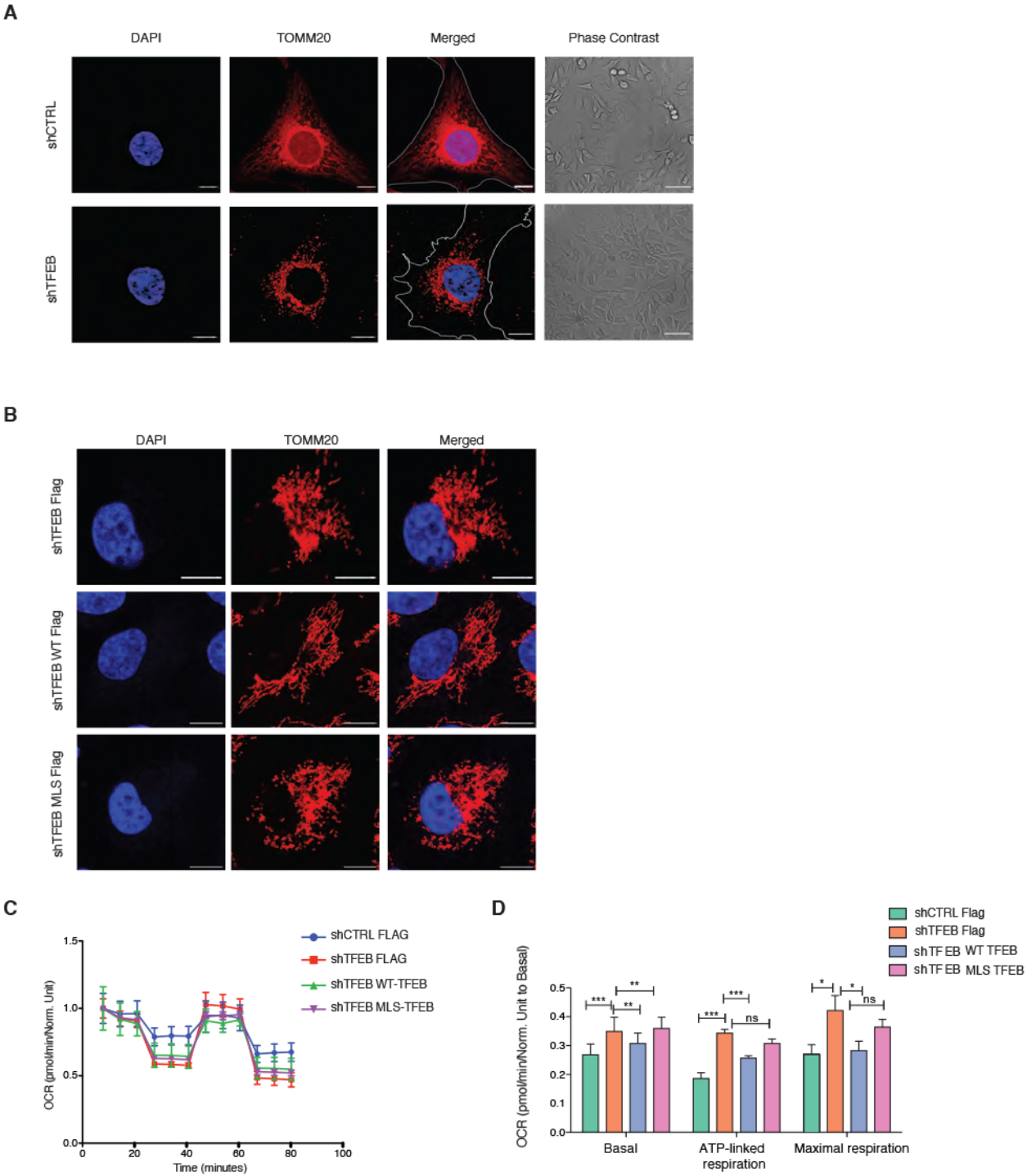
A
DAPI
TOMM20
Merged
Phase Contrast
shCTRL
shTFEB
B
DAPI
TOMM20
Merged
shTFEB Flag
shTFEB WT Flag
shTFEB MLS Flag
C
shCTRL FLAG
shTFEB FLAG
shTFEB WT-TFEB
shTFEB MLS-TFEB
OCR (pmol/min/Norm. Unit)
Time (minutes)
D
shCTRL Flag
shTFEB Flag
shTFEB WT TFEB
shTFEB MLS TFEB
OCR (pmol/min/Norm. Unit to Basal)
Basal
ATP-linked respiration
Maximal respiration
ns

Fig.5

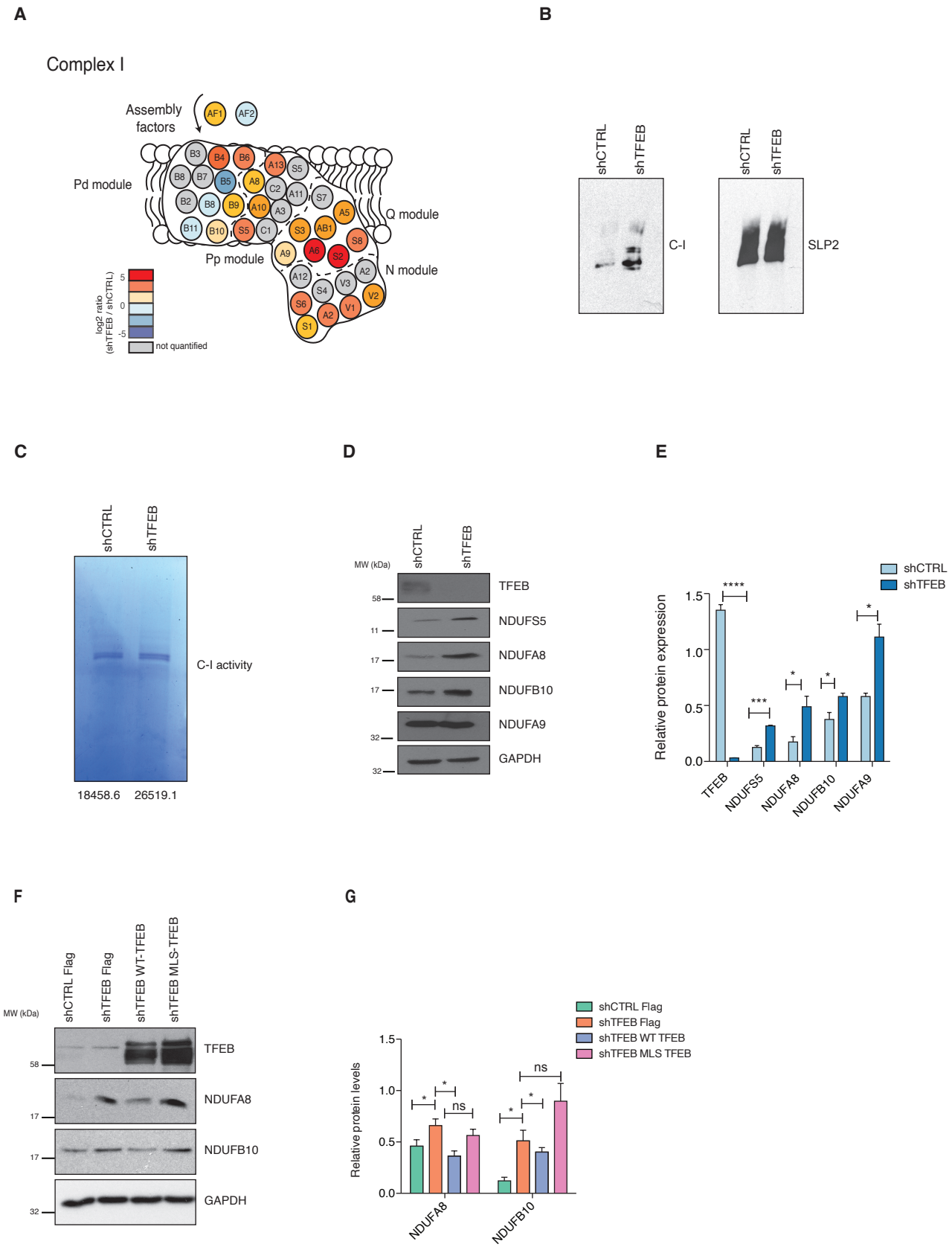
A
Complex I
Assembly factors
AF1
AF2
Pd module
Pp module
Q module
N module
log2 ratio (shTFEB / shCTRL)
5
0
-5
not quantified
B
shCTRL
shTFEB
C-I
SLP2
C
shCTRL
shTFEB
C-I activity
18458.6
26519.1
D
MW (kDa)
shCTRL
shTFEB
TFEB
NDUFS5
NDUFA8
NDUFB10
NDUFA9
GAPDH
58
11
17
17
32
32
E
shCTRL
shTFEB
Relative protein expression
1.5
1.0
0.5
0.0
****
***
*
*
*
TFEB
NDUFS5
NDUFA8
NDUFB10
NDUFA9
F
MW (kDa)
shCTRL Flag
shTFEB Flag
shTFEB WT-TFEB
shTFEB MLS-TFEB
TFEB
NDUFA8
NDUFB10
GAPDH
58
17
17
32
G
shCTRL Flag
shTFEB Flag
shTFEB WT TFEB
shTFEB MLS TFEB
Relative protein levels
1.5
1.0
0.5
0.0
*
*
ns
*
*
ns
NDUFA8
NDUFB10

Fig.6

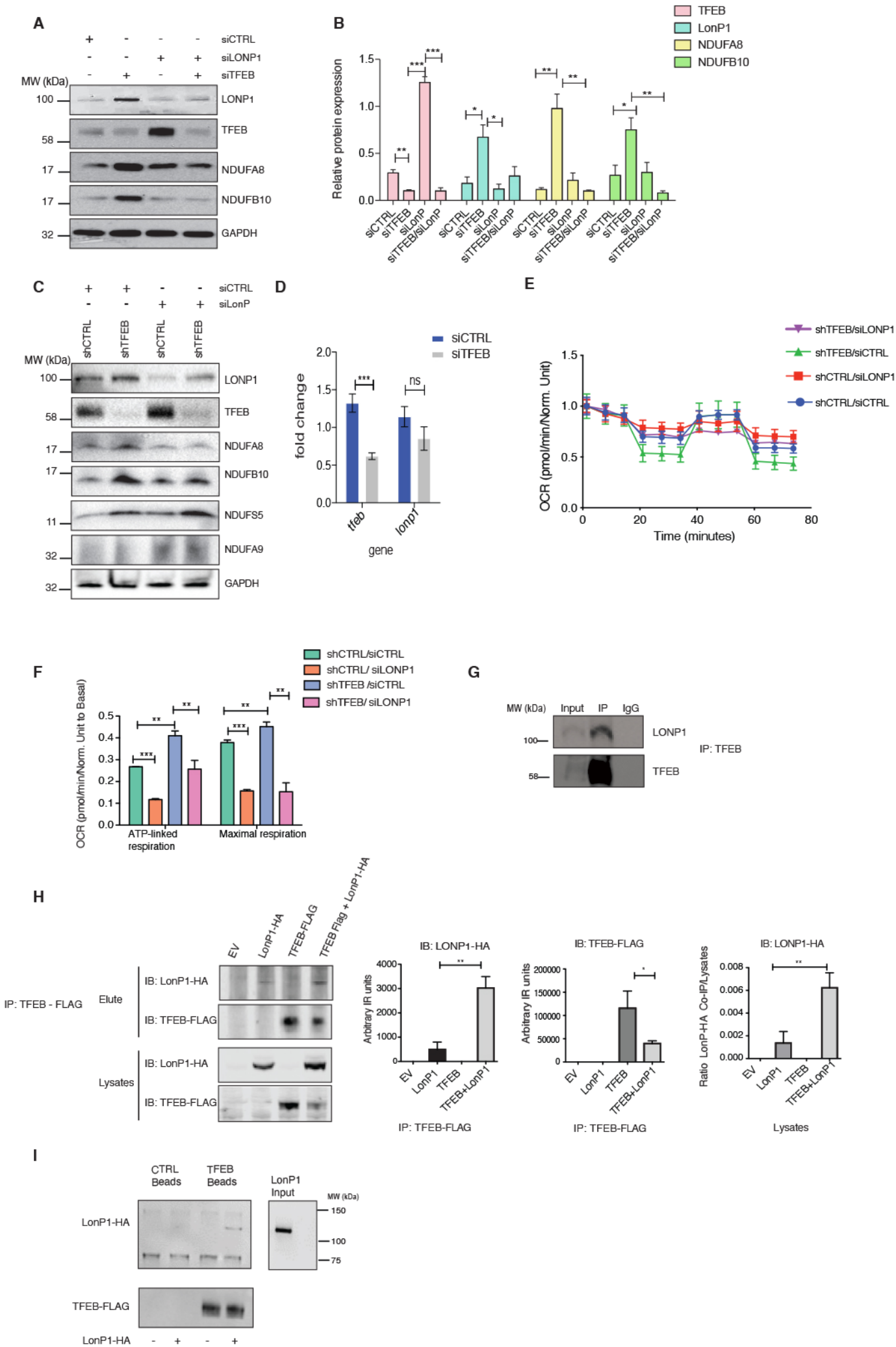
A
siCTRL
siLONP1
siTFEB
MW (kDa)
100
58
17
17
32
LONP1
TFEB
NDUFA8
NDUFB10
GAPDH
B
TFEB
LonP1
NDUFA8
NDUFB10
Relative protein expression
siCTRL
siTFEB
siLonP
siTFEB/siLonP
C
siCTRL
siLonP
shCTRL
shTFEB
11
NDUFS5
NDUFA9
D
siCTRL
siTFEB
fold change
tfeb
lonp1
ns
gene
E
shTFEB/siLONP1
shTFEB/siCTRL
shCTRL/siLONP1
shCTRL/siCTRL
OCR (pmol/min/Norm. Unit)
Time (minutes)
F
shCTRL/siCTRL
shCTRL/ siLONP1
shTFEB /siCTRL
shTFEB/ siLONP1
OCR (pmol/min/Norm. Unit to Basal)
ATP-linked respiration
Maximal respiration
G
MW (kDa)
Input
IP
IgG
LONP1
TFEB
IP: TFEB
H
EV
LonP1-HA
TFEB-FLAG
TFEB Flag + LonP1-HA
IP: TFEB - FLAG
Elute
Lysates
IB: LonP1-HA
IB: TFEB-FLAG
Arbitrary IR units
Ratio LonP-HA Co-IP/Lysates
EV
LonP1
TFEB
TFEB+LonP1
IP: TFEB-FLAG
Lysates
I
CTRL Beads
TFEB Beads
LonP1 Input
MW (kDa)
150
100
75
LonP1-HA
TFEB-FLAG

Fig.7

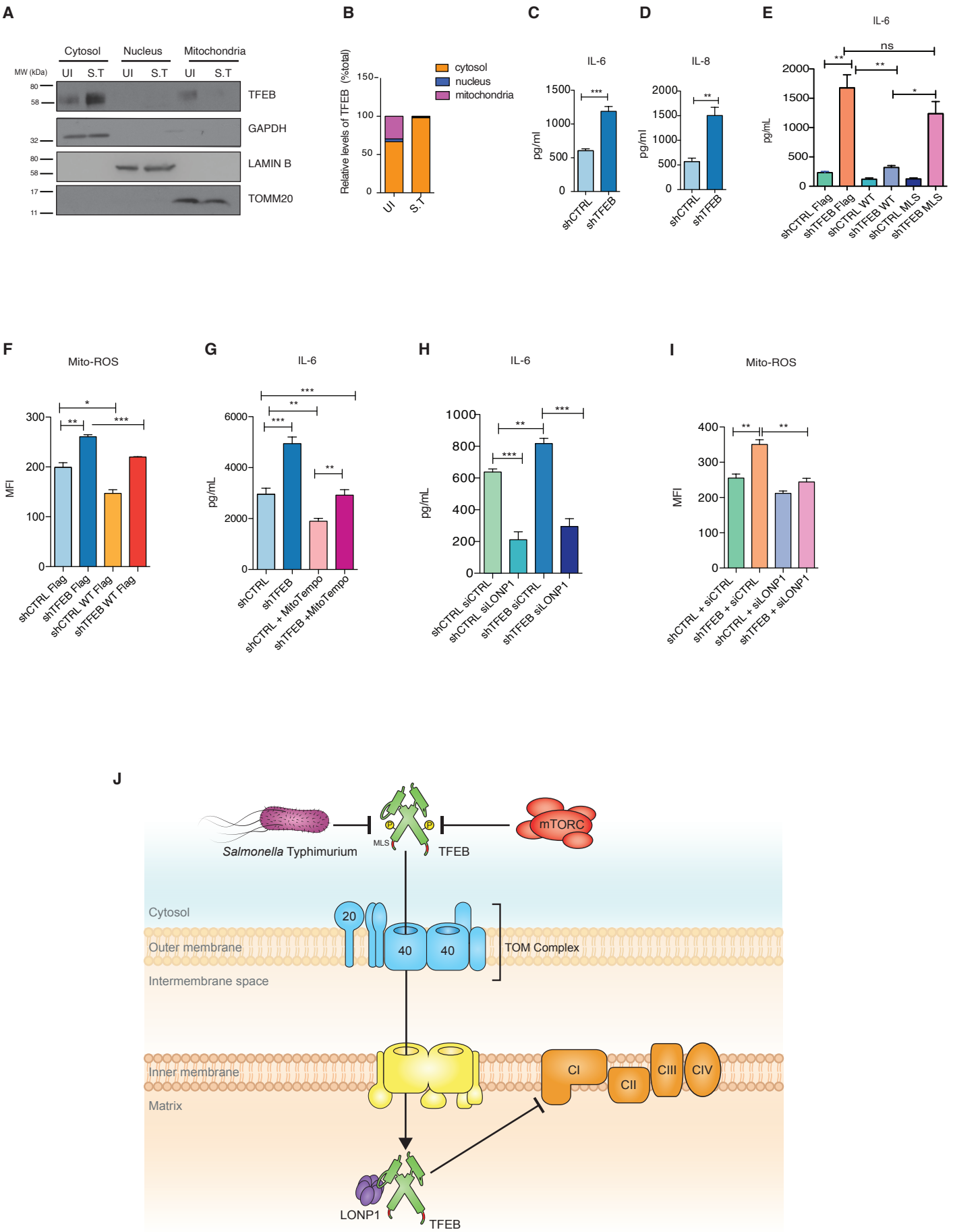
A
Cytosol
Nucleus
Mitochondria
MW (kDa)
UI
S.T
TFEB
GAPDH
LAMIN B
TOMM20
B
Relative levels of TFEB (%total)
cytosol
nucleus
mitochondria
C
IL-6
pg/ml
shCTRL
shTFEB
D
IL-8
E
IL-6
ns
shCTRL Flag
shTFEB Flag
shCTRL WT
shTFEB WT
shCTRL MLS
shTFEB MLS
F
Mito-ROS
MFI
shCTRL Flag
shTFEB Flag
shCTRL WT Flag
shTFEB WT Flag
G
IL-6
pg/mL
shCTRL
shTFEB
shCTRL + MitoTempo
shTFEB +MitoTempo
H
IL-6
pg/mL
shCTRL siCTRL
shCTRL siLONP1
shTFEB siCTRL
shTFEB siLONP1
I
Mito-ROS
MFI
shCTRL + siCTRL
shTFEB + siCTRL
shCTRL + siLONP1
shTFEB + siLONP1
J
Salmonella Typhimurium
MLS
TFEB
mTORC
Cytosol
Outer membrane
Intermembrane space
20
40
40
TOM Complex
Inner membrane
Matrix
CI
CII
CIII
CIV
LONP1
TFEB